coatings

MDPI

Review

Recent Gel Coatings for Electrochemical Protection of Metallic Substrates

Hany M. Abd El-Lateef [1,*] and Ibrahim M. A. Mohamed [2,3,*]

[1] Department of Chemistry, College of Science, King Faisal University, Al-Ahsa 31982, Saudi Arabia
[2] Department of Chemistry, Faculty of Science, Sohag University, Sohag 82524, Egypt
[3] Faculty of Science, Sohag National University, Sohag 82511, Egypt
* Correspondence: hmahmed@kfu.edu.sa (H.M.A.E.-L.); ibrahim_mohamed@science.sohag.edu.eg (I.M.A.M.)

Abstract

Recently, gel coatings have been studied as a promising method that can provide electrochemical corrosion protection. This review presents a comprehensive analysis of advanced gels such as sol–gel coatings, hybrid organic–inorganic, self-healing, and crack repair gels. These gels employ different mechanisms for corrosion protection, from passive barrier formation to active self-healing and corrosion inhibition. Their performance can be influenced by gel chemistry, microstructure, and the incorporation of functional additives. Recent studies have shown that gel coatings can achieve promising corrosion resistance. This high efficiency can be attributed to the formation of dense barrier layers that restrict the mobility of attacking ions. The incorporation of functional additives such as silica nanoparticles can enhance mechanical characteristics for gels. In the field of crack-repair, bio-gels based on microbially induced calcium carbonate precipitation show acceptable sealing capability. Additionally, the evolution of polarization resistance and corrosion current suggests the sustained protective performance of these gels. Multifunctional gels extend this concept by combining crack sealing, alkalinity restoration, and steel re-passivation. Gel coatings are transitioning from simple barrier coatings to multifunctional smart inhibition capable of self-healing, corrosion sensing, and long-term durability. This review highlights the relationship between gel chemistry, microstructure, and corrosion resistance for the development of next-generation gel coatings.

Keywords: polymer gel coatings; corrosion resistance; sol–gel technology; self-healing materials; crack repair gels; hybrid organic–inorganic coatings; electrochemical performance; reinforced concrete; durability enhancement

Check for updates

Academic Editor: Francesco Di Quarto

Received: 9 July 2026
Revised: 28 July 2026
Accepted: 11 August 2026
Published: 13 August 2026

Copyright: © 2026 by the authors. Licensee MDPI, Basel, Switzerland. This article is an open access article distributed under the terms and conditions of the Creative Commons Attribution (CC BY) license.

1. Introduction

Corrosion of metallic substrates in engineering applications remains a persistent challenge across a wide range of energy and industrial fields such as lithium-sulfur batteries [1], solid-state batteries [2], thermoelectric devices [3], solar cells [4], fuel cells [5], and civil engineering [6]. The degradation of metals due to electrochemical interactions with aggressive environments leads to considerable economic losses and safety concerns [7], which encourage researchers to find solutions such as grafting carbon material onto polymer [8] or functionalization of polymers by amino groups [9]. Although the development of corrosion-resistant alloys [10,11] and cathodic protection [12,13] techniques has occurred, the demand for efficient, durable, and low-cost surface protection strategies continues to grow. Among

the studied methods proposed to mitigate corrosion, surface coatings have emerged as one of the most practical and compatible solutions [14].

Traditional organic coatings are widely used because of ease of application and relatively low cost. However, they often suffer from some limitations, such as poor thermal and chemical stability, limited adhesion to metallic substrates under aggressive conditions, and gradual degradation over time. Inorganic coatings can provide acceptable chemical resistance, but with brittleness and processing complexity. These limitations have driven the development of advanced coating systems that combine the advantages of both organic and inorganic materials. In this work, gel-based coatings have attracted significant attention as a promising class of advanced protective materials. Hydrolysis and condensation of metal alkoxides can be used to prepare sol–gels [15] as well as organosilane precursors [16]. This coating can be deposited as thin, uniform films on metallic substrates. This approach enables control over the chemical composition and microstructure of the resulting coatings to design an effective layer against electrochemical corrosion. Figure 1 shows the number of publications on polymer gel corrosion manuscripts collected from the Scopus database with the words Polymer + Gel + Corrosion in the title, abstract, or keywords of the published manuscripts in the Scopus database. The data show a stable number of research publications between 2011 and 2020. Then, it increased gradually from 2021 to 2024, which can reflect the emergence of advanced gel systems such as hybrid, nanostructured, and self-healing coatings. Therefore, the trend highlights sustained scientific interest in gel-based corrosion protection technologies.

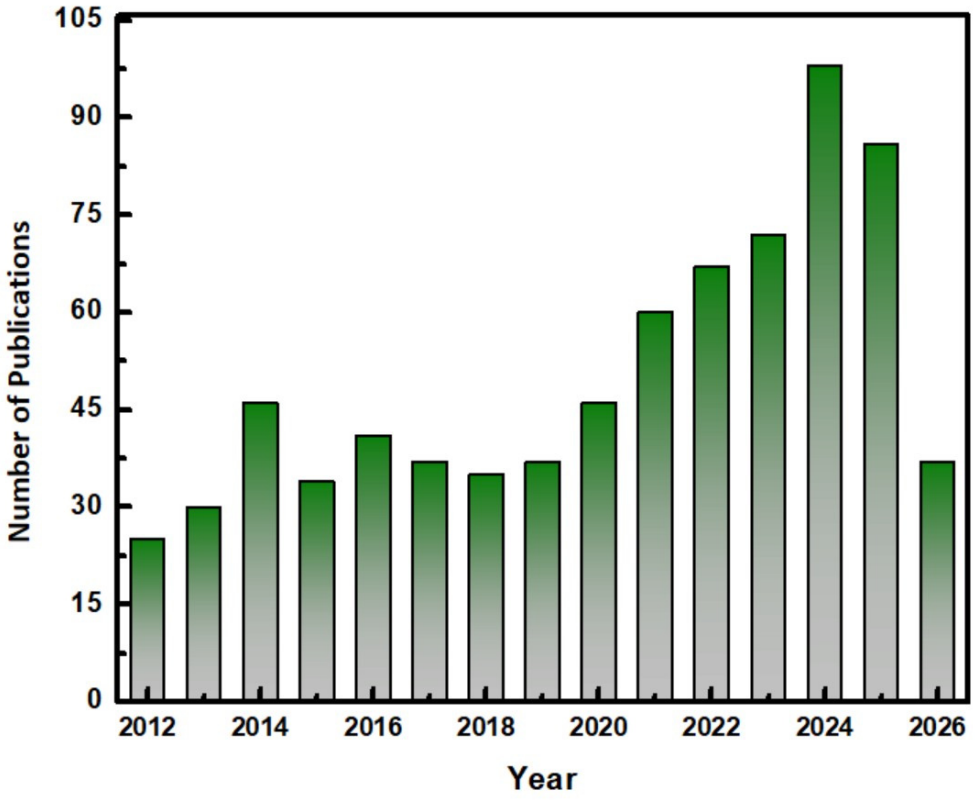


Figure 1. Number of publications on polymer gel corrosion studies (Scopus search using Polymer + Gel" + "Corrosion" words in the title, abstract, or keywords of manuscripts). The publication data for 2026 corresponds to the records available in the Scopus (Elsevier) database up to May 2026.

One of the advantages of gel-based coatings is chemical versatility [17–20]. The sol–gel process can be carried out in low-temperature fabrication [21,22], is compatible with a wide range of substrates, and allows for the incorporation of functional additives [23,24]. So,

these coatings can provide both passive protection through barrier effects and reduced permeability [25] in addition to active protection mechanisms such as inhibitor release [26,27]. The performance of such coatings can be influenced by the structure of the gel network, which is governed by synthesis parameters such as precursor chemistry and pH. So, an introduction to the advances of sol–gel chemistry for corrosion inhibition is needed. Over the past decades, extensive research has been conducted to improve corrosion resistance via gel coatings of some metallic substrates such as steels [28,29], magnesium alloys [30–32], Zn-Cu-Ti alloy [33], aluminum alloys [34–36], fragile bronze [37], and other engineering or industrial metals. Improved performance has been attributed to different mechanisms such as enhanced barrier properties, improved adhesion, and increased hydrophobicity. Hybrid polymer gels show considerable promise by combining the flexibility of polymeric components and durability. Although polymer gel shows promising behavior, several scientific issues limit the industrial use of gels. These demerits include issues related to shrinkage and cracking during drying and long-term usage. Therefore, there is a need for a deeper understanding of the relationships between gel chemistry, microstructure, and corrosion protection performance [38,39]. Addressing these challenges is essential for the development of coating systems. Therefore, this review presents an overview of polymer gel coatings for corrosion resistance of metallic substrates. Finally, key challenges and future research directions are mentioned to provide the correct pathway for research groups working on this issue. Although several review articles have discussed specific aspects of sol–gel, most are limited to individual materials or particular protection strategies. This review introduces broader and more integrative concepts by discussing recent gel-based corrosion-protective coatings such as conventional sol–gel systems, polymer-gel composites, nanostructured and MOF-based coatings, self-healing materials, bio-inspired and plant-derived gel systems, and sustainable coating technologies. In addition, this review compares protection mechanisms, correlating coating composition with electrochemical performance. Additionally, it discusses durability, limitations, research trends, and future opportunities. This integrated and critical perspective provides researchers with a comprehensive framework for understanding the current state and future development of gel coatings for metallic substrate protection.

2. Fundamentals of Gels

2.1. Chemistry of Gels

Sol–gel chemistry is fundamentally governed by the hydrolysis and condensation reactions of metal alkoxides. These alkoxides drive the transformation from molecular species into the inorganic or hybrid network [40]. For example, tetraethyl orthosilicate (TEOS) and titanium alkoxides can undergo hydrolysis to produce reactive silanol (Si-OH) and metal hydroxyl (Ti-OH) bonds. Then, it goes to condensation into M-O-M bonds, such as Si-O-Si, Ti-O-Ti, and hetero-linkages (Si-O-Ti). The formation of these bonds can be indicated through FT-IR analysis at 1086 cm^{-1}, 951 cm^{-1}, and 466–613 cm^{-1} for Si-O-Si, Si-O-Ti, and Ti-O-Ti, respectively [41]. This form of molecular network governs the structural continuity and the barrier properties of the coating. This method forms a transformation at low temperatures and can form a TiO_2-SiO_2 multilayer to be utilized as corrosion-protective layers. The corrosion resistance is improved with more coating layers. The highest corrosion resistance of 61 kΩ cm^2 was obtained for the three-layer coating [41]. The chemical kinetics of hydrolysis and condensation reactions depend upon synthesis parameters, especially the acidity environment (pH), as well as precursor ratios and catalytic species. An acidic environment promotes controlled hydrolysis and delayed condensation, which gives homogeneous sols suitable for coating deposition. In contrast, the introduction of basic catalysts such as triethylenetetramine (TETA) can accelerate con-

densation reactions [42]. From a molecular perspective, the pH of the sol influences the balance between hydrolysis and condensation reactions and therefore determines the final gel characteristics [43]. Under acidic conditions, hydrolysis of metal alkoxides is favored, producing a high concentration of reactive silanol (Si-OH) groups while condensation proceeds relatively slowly [15]. This controlled reaction pathway increases the gradual formation of siloxane (Si-O-Si), which can give a homogeneous and highly crosslinked network with low porosity and fewer structural defects. In contrast, under alkaline conditions, deprotonated silanol species have higher nucleophilicity, which accelerates condensation reactions. Although rapid Si-O-Si bond formation shortens gelation time, it can produce heterogeneous networks with localized aggregation, larger pores, and internal stresses that can lead to microcrack formation. So, gels prepared under optimized acidic conditions generally exhibit higher crosslinking density, lower electrolyte permeability, and superior corrosion resistance because the compact siloxane network can restrict the transport of aggressive ions toward the metallic substrate. Quantitative NMR studies reveal that condensed siloxane species become dominant within 30–60 min depending on TETA concentration. This fast condensation shortens gelation time from >90 days in uncatalyzed systems to less than 1–2 h because of TETA. This indicates the catalytic effect of amine functionalities. However, this acceleration comes at the expense of sol stability, which can retard processability in commercial coating applications. A central feature of gel coatings is the formation of organic–inorganic networks. A clear example is the formation of organofunctional silanes from 3-glycidoxypropyl trimethoxysilane (GPTMS) [42]. The chemistry of formation is based upon inorganic condensation and organic polymerization to form hybrid structures with covalent interconnections. Experimental evidence shows that epoxy-amine reactions are exothermic (100–118 kJ per equivalent epoxy), which is over the hydrolysis enthalpy (12.9 $kJ \cdot mol^{-1}$ for TEOS). The polymerization of the organic content can decrease the growth of the siloxane network. So, there is a complex interplay between flexibility and crosslink density. Solid-state NMR analyses indicate that fully cured systems exhibit high condensation levels. This competition between organic and inorganic content is a key factor controlling mechanical and corrosion resistance.

2.2. Processing Parameters of Gels

Gel chemistry defines the fundamental reactions governing the formation of gel networks, while the processing parameters of gels can determine how this chemistry converts into functional coatings. These parameters include pH, aging time, deposition conditions, thermal treatment, layer architecture, and substrate pretreatment, as shown in Table 1. These parameters can control the formation of microstructure, porosity, and interfacial bonding, which have a considerable impact on corrosion performance [38,44]. Therefore, understanding the processing–structure performance relationship is essential for optimizing protective gel coatings. Direct deposition of acidic sols can lead to poor adhesion. To mitigate this, fluoride-based pretreatments are employed to create a stable intermediate layer. Experimental studies demonstrate that increasing pretreatment time (from 1 h to 120 h) results in thicker hydroxyfluoride layers (600–900 nm) with higher fluorine content [45]. This interfacial layer significantly improves corrosion resistance, which was indicated via the decrease in current density from 17.8 $\mu A \cdot cm^{-2}$ to 1.84 $\mu A \cdot cm^{-2}$ after pretreatment, and decreased again to 0.0137 $\mu A \cdot cm^{-2}$ when combined with a sol–gel coating. Previously, gels were prepared under different pH values from 1 to 10, followed by coating on AA2024-T3 [38]. The viscosity and particle size results suggest that the condensation shows an order of pH = 4 > 1 > 7 > 10. After corrosion resistance tests, it is found that the protection efficiency of the formed gel is in the same arrangement (pH = 4 > 1 > 7 > 10). A high condensation degree could increase the formation of the compact gel coating with high

crosslinking density and less silanol content. Additionally, too high a condensation degree can lead to turbidity in the sol synthesis process. The transition from gel to dense coating involves physicochemical transformations during drying and thermal treatment. Thermogravimetric analysis of TiO_2-SiO_2 gels reveals a total mass loss of 75% because of solvent evaporation and removal of residual organics, followed by decomposition steps between 200 and 425 °C associated with residual alkyl groups [41]. These processes are accompanied by endothermic characteristics around ~125 °C and ~250 °C because of solvent removal and organic decomposition, respectively. Above these temperatures, condensation reactions dominate, followed by formation of stable oxide networks. This thermal evolution directly affects porosity and microstructure. Increasing annealing temperature from 700 °C to 900 °C promotes grain growth and the formation of dense coatings with thicknesses of 3–4 µm. The effectiveness of sol–gel coatings for corrosion protection is linked to the degree of network condensation, homogeneity, and chemistry. Dense, highly crosslinked networks act as effective barriers against ionic diffusion. For example, TiO_2-SiO_2 multilayer coatings derived via optimized sol–gel processing exhibit an increase in polarization resistance from 2 kΩ·cm^2 to 61 kΩ·cm^2 after annealing at 900 °C in air. Similarly, the gel coatings incorporating TETA show impedance values on the order of 10^5–10^6 Ω·cm^2. This reflects promising barrier properties compared to non-modified systems [42]. These enhancements can be due to increased crosslink density, and the formation of a stable oxide-silicate structure. On the other hand, excessive densification with fast condensation can facilitate internal defects, which indicates the need for control over processing parameters to achieve the optimum corrosion resistance.

Table 1. Processing parameters, conditions, structural effect and corrosion performance of the reported gels.

Processing Parameter	Condition	Structural Effect	Corrosion Performance	Reference
pH (during preparation)	2–3	Controlled hydrolysis, homogeneous sol	Improved coating uniformity	[41]
Aging time	24–168 h	Increased network connectivity	Reduced cracking, better barrier	[41,45]
Number of layers	one to three	Increased thickness, defect healing	Rp increased from 2 to 61 kΩ·cm^2	[41]
Annealing temperature	700 to 900 °C	Densification, pore coalescence		
Pretreatment time (Mg)	1 to 24 h	Formation of compact hydroxyfluoride layer	Corrosion current decreased to 1.37×10^{-8} A·cm^{-2}	[45]
Excess pretreatment	>24 h	Nanoparticle agglomeration, defects	No further improvement	[45]
Deposition rate	Controlled (2.5 mm/s)	Uniform thickness (1.5 µm)	Stable barrier	[45]

2.3. Structural Evolution of Gels

The structural evolution of gels is a dynamic process that bridges gel chemistry and processing parameters. During deposition, the formed gel undergoes transformations driven by solvent evaporation, condensation reactions, and thermal treatment. Drying removes physically adsorbed solvent molecules and induces capillary stresses, which can lead to shrinkage and microcrack formation. As temperature increases, condensation enhances gel network connectivity, and the gel becomes a dense, crosslinked structure with reduced porosity. For instance, TiO_2-SiO_2 coatings exhibit a transition from nanoporous films at 700 °C to compact layers at 900 °C [41]. This densification is correlated with corrosion resistance, as suggested by the increase in resistance from the order of 10^3 Ω·cm^2 for an uncoated substrate to 10^4–10^5 Ω·cm^2 for optimized coatings. Structural evolution plays an additional role by governing the distribution, encapsulation, and release behavior

of active species. Furthermore, interfacial evolution enhances adhesion and provides an additional barrier against corrosion. Therefore, structural evolution in gel coatings is not merely a consequence of processing but a critical design parameter that must be carefully studied to balance mechanical, barrier properties, and functional responsiveness for advanced corrosion protection systems.

Structural evolution in gel systems should be understood as a multiscale process involving molecular condensation, pore-network rearrangement, bonding, and transport behavior. Chen et al. showed that the pH of sol synthesis strongly affects the structural development of silane-zirconium sol–gel coatings: the pH = 4 system exhibited the highest condensation degree and the greatest Si-O-Si contribution of 71.8%, while the pH = 10 coating had only 40.23% Si-O-Si and 30.54% Si-OH [38]. This structural difference impacted corrosion performance. The usage of pH 4 coating showed the highest charge-transfer resistance of 8.42×10^5 $\Omega \cdot cm^2$ with an only 3.2% damaged area after 960 h in 3.5% NaCl compared with 54.9% for the use of pH 10 coating. Additionally, Mahadevan et al. demonstrated through reactive molecular dynamics that gel evolution is controlled via chemical condensation and hydration reorganization, silanol/aluminol formation, pore-size redistribution, and water-transport restriction [46]. Their simulations showed that increasing temperature from 298 to 363 K accelerated silanol and aluminol formation. This can promote pore restructuring and reduced water diffusivity inside gel networks to 0.03–0.086 $Å^2/s$ at 298 K and 0.08–0.18 $Å^2/s$ at 363 K, compared with 0.24 $Å^2/s$ for bulk water. Therefore, these studies indicate that effective corrosion-protective gel coatings require a controlled structural evolution that maximizes network condensation and interfacial bonding while minimizing pathways for electrolyte transport [38,46].

2.4. Deposition Fundamentals of Gels and Time-Resolved Evolution

The deposition of gels represents a critical stage in experimental work because it has a considerable impact on the physicochemical properties and the formation of a functional protective film. Among the available techniques, dip coating remains the most reported method for corrosion protection applications because of its simplicity and ability to produce uniform thin films [47,48]. Figure 2 illustrates the glow discharge optical emission spectroscopy (GD-OES) depth profiles of Zn, Si, C, and Fe. This can provide insight into the compositional distribution and thickness evolution of gels deposited on hot-dip galvanized steel (HDGS) substrates. An organic–inorganic film can be indicated via the distinction between the coating layer and the zinc substrate. The coating thickness increases with the number of deposited layers. It was found to range from 2 μm for a single layer to about 17–18 μm for three-layer systems. This represents a ninefold increase and indicates the dependence of coating layer on sequential deposition [47]. The impact of residence time (Rt) on thickness is small. Coatings prepared with Rt = 0 s and Rt = 100 s have similar thickness values (17 μm and 18 μm for three layers). This confirms that Rt cannot contribute to mass deposition. From a corrosion protection overview, these thickness variations are relevant. The increase in thickness enhanced the diffusion path for aggressive species. However, optimizing processing parameters such as curing may be more impactful than residence time. Therefore, the depth profile analysis demonstrated that controlled multilayer deposition with adequate curing is essential for achieving a robust and effective gel.

Additionally, the time-resolved evolution of the corrosion product layer resistance (RL) and the open circuit potential for zinc surfaces with different initial states (pickled, as-received, and long-term exposed) were investigated as displayed in Figure 3 [49]. Pronounced transient behavior was observed after contact with the gel (within 2–3 min). RL increased sharply before reaching a quasi-steady state after 10–15 min. Quantitatively, the long-term exposed sample has higher resistance in the range of 314–370 $k\Omega \cdot cm^2$, whereas

the pickled samples have lower values (16 kΩ·cm^2). This difference indicated the protective nature of the corrosion products formed during atmospheric exposure. The initial increase in RL can be attributed to the fast formation of a thin electrolyte film. As the system stabilizes, the resistance increase reflected the intrinsic barrier properties of the corrosion product layer. The relatively stable RL values over time suggest that the gel does not disrupt the surface. From a mechanistic view, this dynamic measurement provides insight compared to single-point electrochemical techniques. It can capture both the wetting kinetics and the early-stage electrochemical response of the surface. Therefore, the serial RL approach offers a sensitive tool for distinguishing between unstable, thin surface films and well-developed, protective corrosion layers [49].

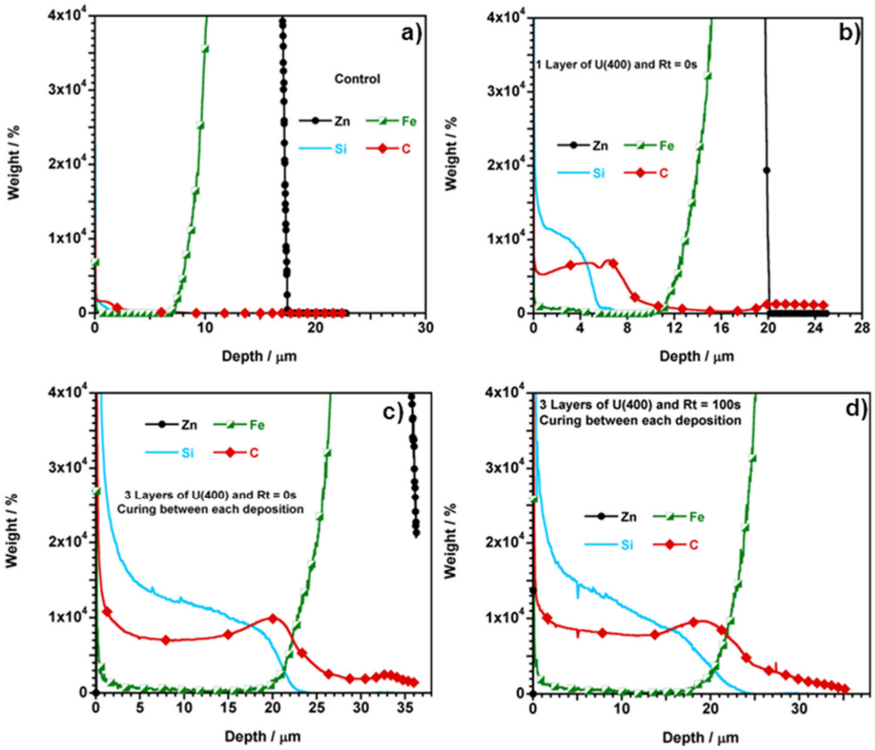


Figure 2. Detailed view of the GD-OES depth profiles for Zn, C, Fe and Si within HDGS substrates for (**a**) control; (**b**) one layer of U(400) and Rt = 0 s; (**c**) three layers of U(400) with cures between each deposition and Rt = 0 s; (**d**) three layers of U(400) with cures between each deposition and Rt = 100 s. Reproduced from Figueira et al. (2015) [47] under CC BY license.

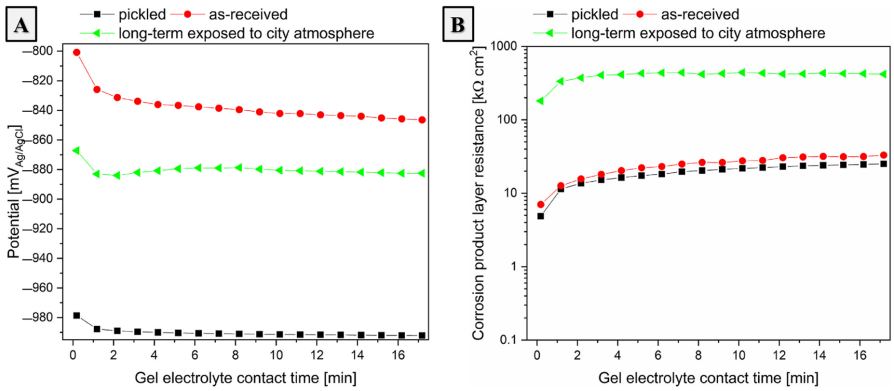


Figure 3. Series measurements of (**A**) the corrosion potential and (**B**) the corrosion product layer resistance (R_1) of pickled, as-received, and long-term exposed zinc surfaces during gel-electrolyte contact for up to 17 min. Reproduced from Valet et al. (2021) [49] under CC BY license.

3. Hybrid and Organic–Inorganic Gel Coatings

3.1. Hybrid Silica Gels

Hybrid silica-based gel coatings are among the developed sol–gels reported for metallic corrosion protection because they have a condensed Si-O-Si network with organic content that reduces cracking, improves flexibility, and enhances adhesion [50–52]. Their protection depends upon the formation of a dense barrier layer, stable interfacial M-O-Si bonding, and suppression of electrolyte transport. However, the attached studies show that corrosion inhibition depends strongly on polymerization atmosphere, curing degree, hydrophobicity, inhibitor loading, and secondary oxide incorporation. For MMA/MAPTMS/TEOS coatings on AA2024-T3, Rodič et al. showed that oxygen-free copolymerization under nitrogen produced smoother 4 μm coatings and much better long-term protection than air-prepared coatings [53]. The optimized MMT-N_2 coating reached impedance values close to 1 GΩ cm^2 after 6 months in 0.1 M NaCl. In contrast, salt-spray testing showed no visible damage after 500 h; by contrast, bare AA2024-T3 showed corrosion products after only 6 h and was completely covered after 300 h. In hybrid silica coatings, corrosion resistance can be improved when the inhibitor is compatible with the gel network. Suarez-Vega et al. incorporated Lanthanum 4-hydroxy cinnamate La(4-OHCin)$_3$ into TEOS/GPTMS/BPA-based coatings on carbon steel [54]. The silica network provided the passive barrier, while the lanthanum-cinnamate inhibitor added active corrosion inhibition by retarding anodic and cathodic reactions. The study showed that inhibitor concentration can be optimized because excessive loading can increase roughness, porosity, and defect formation, which reduce barrier efficiency [54].

Zr-modified silica gels also show promising performance. Nguyen et al. reported TEOS/MAPTMS/Zr hybrid coatings on hot-dip galvanized steel with initial low-frequency impedance around 10^7 Ω cm^2 and changed after 24 h in 0.1 M NaCl to 5×10^6 Ω cm^2 within 72–168 h. Cerium nitrate addition improved active protection in the presence of 650 ppm Ce(III), which is the optimal concentration. Higher Ce contents increased viscosity and reticulation but could have compromised coating quality [55]. Hydrophobic silica hybrids provide another strategy for inhibition. Zhou et al. developed TEOS-polybenzoxazine coatings only 0.5 μm thick. The optimized TEOS-PBz-210 coating achieved a water contact angle of 105.6 ± 0.4° and an R_{ct} above 10^5 Ω cm^2 after 1 week in 3.5% NaCl. This value is one order of magnitude higher than conventional TEOS-GPTES coatings. This performance was linked to 94% benzoxazine conversion, dense crosslinking, and reduced water uptake [36]. Therefore, hybrid silica coatings can be discussed not simply as passive SiO_2-like layers but as tunable organic–inorganic networks. The best corrosion inhibition is obtained when silica condensation, organic crosslinking, inhibitor release, hydrophobicity, and substrate bonding are balanced. The impedance can reach 10^5–10^9 Ω cm^2, corrosion resistance can persist for hundreds of hours in salt spray, and optimized inhibitor or curing conditions can shift performance by more than an order of magnitude.

3.2. ORMOSIL Coatings

A representative class of organic-modified silicate (ORMOSIL) coatings is based on siloxane–polyacrylic hybrid networks [56]. This includes coupling between hydrolyzed silanes and polymerizable acrylate monomers to produce an interpenetrating organic–inorganic structure. These systems can be prepared via (i) radical copolymerization between MAPTMS and acrylate derivatives, (ii) hydrolysis/condensation of TEOS, and (iii) co-condensation between both sols to form a hybrid ORMOSIL network [57]. This structure has siloxane surrounded by organic polyacrylate contents, which provides homogeneous coatings with strong adhesion. The structure–property relationships in these ORMOSIL coatings can be governed by the nature and length of the acrylate side chains.

Experimental results showed that the degree of copolymerization increases from methyl to butyl derivatives and then reaches the highest in longer chains because of steric hindrance. This directly influences wettability. Coatings with short alkyl chains have water contact angles of 70–85°, while perfluoroalkyl-functional coatings reach 90°. This data reflected enhanced hydrophobicity. However, increasing chain length can increase coating porosity. These structural characteristics directly influence corrosion performance. Electrochemical impedance spectroscopy in 5% NaCl over 18 months revealed that coatings containing ethyl (E) and butyl (B) derivatives exhibit the highest corrosion resistance. The impedance values were found around 10 G$\Omega \cdot cm^2$ at low frequency (5 mHz) with phase angles approaching −90°. In contrast, coatings with shorter methyl chains show progressive degradation, evidenced by a decrease in phase angle to −12° after 18 months. Additionally, salt spray testing up to 550 h confirmed the durability of optimized ORMOSIL compositions. Substitution with perfluoroalkyl groups enhances hydrophobicity and copolymerization kinetics but does not significantly outperform short alkyl systems in corrosion resistance [57].

There are some effective strategies that were used to develop ORMOSIL coatings [58–60]. From these strategies, the incorporation of functional organic molecules into silane-based networks is a promising one for corrosion inhibition. This strategy can achieve barrier protection and active corrosion inhibition. Balaji et al. studied p-aminothiophenol (PATP)-modified (3-glycidoxypropyl)trimethoxysilane (GPTMS) coatings [61]. This gel matrix was formed through acid hydrolysis and condensation of GPTMS and PATP, which chemically interact with the silane network and the metallic substrate. The amine group of PATP induces epoxy ring opening of GPTMS, which enhances crosslinking, and the thiol group forms Cu-S bonds at the copper surface. This can lead to a densely packed, chemically anchored ORMOSIL layer. Electrochemical behavior, such as Nyquist and Bode plots, was studied to indicate the beneficial effect of PATP incorporation. Bare copper exhibits a depressed capacitive loop followed by a Warburg tail, which can be used as an indicator of active corrosion. Interestingly, both GPTMS and PATP-GPTMS coatings decrease the Warburg response, which confirms the blocking of some diffusion pathways. Additionally, the diameter of the Nyquist semicircle and the impedance modulus increase with PATP concentration (0.001–0.1 M). This reflects a rise in charge transfer resistance (R_{ct}). The Bode plots further reveal higher impedance values and phase angles for PATP-modified coatings. With 0.1 M PATP-GPTMS, the Bode behavior approaches near-ideal capacitive behavior. The optimized coating exhibits promising inhibition performance and achieves 95.5% efficiency based on EIS and up to 96.39% from polarization measurements in 3.5% NaCl after 12 h. This improvement is attributed to the synergistic effect of (i) a compact Si-O-Si network that limits electrolyte penetration, (ii) increased coating thickness, and (iii) chemisorption via Cu-S bonds [62] that stabilizes the metal/coating interface and decreases anodic dissolution. Therefore, ORMOSIL coatings can be enhanced by molecular-level functionalization through combination with organic inhibitors within the silane network towards multifunctional corrosion protection [61].

A more fundamental understanding of ORMOSIL coatings originates from studies that correlate chemical structure with corrosion performance. Perrin et al. studied GPTMS/TEOS gels crosslinked with multifunctional amines such as triethylenetetramine (TETA) [42]. In these hybrids, simultaneous formation of siloxane (Si-O-Si) and epoxy-amine networks generates an interpenetrating structure. Increasing TETA content accelerates condensation and reduces gelation time from >90 days (without TETA) to <1–2 h. This dual role of TETA (catalyst and crosslinker) leads to a non-linear relationship between structure and performance. Mechanically, the coating depends on crosslinking density: the epoxy-rich formulation (NH/epoxy = 0.5) shows the highest Persoz hardness, correlating with a more developed siloxane network. Excess amine (NH/epoxy = 3) introduces dan-

gling chains and reduces mechanical properties. Additionally, the incorporation of TETA improves the initial barrier properties, with impedance modules at low frequency (10 mHz) reaching 10^5–10^6 Ω·cm^2. This value is approximately one order of magnitude higher than coatings without TETA [42]. In short, corrosion protection is not solely dictated by the degree of crosslinking but by achieving a balance between organic network formation, siloxane condensation, and interfacial reactivity.

3.3. Polymer-Gel Composites

Polymer-gel composite coatings represent an advanced evolution of sol–gel systems [63–65]. They include the incorporation of highly crosslinkable organic polymers such as benzoxazine (Bz) and epoxy (EP) into the inorganic siloxane network, generating multifunctional hybrid gel. Song et al. studied Bz/EP-modified sol–gel coating (SG-PBE) to form a dense multi-crosslinked network through simultaneous Si-O-Si condensation and ring-opening polymerization of oxazine and epoxy groups [66]. The formed polymer-gel hybridization enhances barrier and functional performance compared to traditional sol–gel coatings. Electrochemical results show that optimized composites (SG-PBE180) maintain low-frequency impedance values exceeding 10^6 Ω·cm^2 after 30 days of immersion. Highly crosslinked systems reached values above 10^8 Ω·cm^2, which indicates better corrosion resistance. Increasing crosslinking improves mechanical characteristics and reduces water uptake. Water absorption decreased to 1.29% after 1 day for highly cured coatings. Excessive curing leads to higher intermolecular hydrogen bonding (up to 29.8%) and increased water uptake (7.91% after 28 days) [66]. Therefore, polymer-gel composites demonstrate that optimal performance is achieved not at maximum crosslinking but through controlled hybrid network design.

A polymer-gel composite based on imidazole-core polybenzoxazine–silica hybrids was reported for corrosion and flame resistance [67]. It includes a crosslinked polymer network and a reinforcing Si-O-Si framework. The curing behavior of the benzoxazine precursor shows a reduced polymerization temperature. The curing initiated at 174 °C and peaked at 200 °C, which is lower than traditional systems (264 °C). This can indicate the facilitation of efficient network formation. The incorporation of silica (TEOS/HDTMS, 0%–40%) improves thermal stability, which was evidenced by an increase in initial degradation temperature from 234 °C to 265–286 °C. The polymer-gel composite has remarkable surface and barrier properties. Hydrophobicity increases significantly with silica modification, with water contact angles rising from 125° for neat polymer to 140° for 40% HDTMS systems. This reflects reduced surface energy and improved water repellence. This structural evolution influences corrosion resistance. Electrochemical impedance results show an increase in charge transfer resistance from 9 Ω·cm^2 to 856 Ω·cm^2 and up to 28,563 Ω·cm^2 for bare steel, polymer, and optimized composites, respectively. Low-frequency impedance reaches 9.2×10^7 Ω·cm^2 for HDTMS coatings. Long-term immersion tests confirmed durability, with HDTMS-based systems maintaining impedance values of 9.1×10^7 Ω·cm^2 even after 14–21 days. Additionally, corrosion inhibition efficiency reaches 98.47%. This is accompanied by a positive shift in corrosion potential from −885.80 mV (bare steel) to −450.76 mV [67]. Therefore, polymer-gel composites achieve superior performance through a finely tuned synergy between polymer crosslinking, silica reinforcement, and surface hydrophobicity.

Recent advances in polymer composites have also demonstrated the potential of supramolecular engineering to enhance the structural and functional properties of polymeric materials. Mechanically interlocked molecules, such as homo-2-catenane fillers, can establish reversible supramolecular crosslinking through strong π–π and electrostatic interactions with polymer chains [68]. This structure forms denser polymer networks

with improved mechanical and functional characteristics. Although this strategy has been studied for energy storage, it provides insights into the rational design of multifunctional polymer composite coatings, where supramolecular interactions may improve network integrity, durability, and long-term stability. Additionally, eco-friendly polymer-gel composite coatings were studied for corrosion inhibition based on waterborne polyurethane (WBPU), catecholamine-modified sol–gel interlayers [69]. The introduction of a catecholamine (CAm/MPD) layer improved adhesion strength. The dry adhesion increased from 1.74 MPa to 2.75 MPa, and wet adhesion increased from 1.15 MPa to 3.70 MPa after prolonged exposure. This indicated strong interfacial bonding inspired by chemistry content. EIS results reveal improvements in barrier properties. The charge transfer resistance increased from 4.9×10^4 Ω·cm^2 to 1.7×10^7 Ω·cm^2 after 120 days of immersion in 3.5% NaCl. This is an enhancement of more than two orders of magnitude. Similarly, low-frequency impedance values for optimized WBPU/CM@sol-gel coatings reached 4.7×10^6 Ω·cm^2 after 120 days, and lower values were found at 6.8×10^4 Ω·cm^2 and 6.9×10^5 Ω·cm^2 for unmodified and polydopamine (PDA)-based systems, respectively. The CAm/MPD@sol-gel coatings have optimal concentrations (2–4 mg/mL) as they maintain impedance values above 10^6 Ω·cm^2 for at least 49 days. Structurally, AFM analysis shows a reduction in surface roughness from 9.901 nm to 1.120 nm, while SEM/EDS cross-sections indicate a uniform interlayer thickness of approximately 9.5 ± 0.2 µm. This can indicate enhanced compactness and defect filling. These improvements are attributed to the nano-crosslinked structure of CAm/MPD that infiltrates and seals sol–gel micropores to form a dense hybrid network that effectively blocks chloride ions and water. In short, polymer-gel composite coatings achieve promising corrosion protection through the combined effects of enhanced adhesion and reduced porosity for protection of reactive Mg alloys [69].

4. Gel-Based Composite and Nanostructured Coatings

Gel-based composites combined with nanostructured coatings represent a promising class of advanced protective systems [70–72]. Although some composite gels discussed in this review may be classified as both polymer-gel composites and gel-based nanostructured coatings, these sections are distinguished according to their primary design strategy. Section 3.3 discusses the polymer-gel composites, where the polymer gel has the continuous matrix and other components may be incorporated to improve mechanical integrity, adhesion, barrier properties, and corrosion resistance. In contrast, this section discusses gel-based composites and nanostructured coatings in which nanoscale fillers, hierarchical structures, and hybrid inorganic–organic architectures are the dominant design features. Unlike rigid coatings, these systems exploit flexibility, porosity, and tunable chemistry of gel networks [73,74]. These characteristics can enhance both passive barrier properties and active corrosion protection mechanisms. Examples of nanostructures that can be incorporated in gels are inorganic nanoparticles [75], carbon-based nanofillers [76] including CNTs [77], graphene [78], nanodiamonds [79,80], and hybrid frameworks such as MOFs [81–83] and metal–organic gels (MOGs) [84,85]. The combination of gel networks and nanoparticle characteristics can improve dispersion, defect sealing, and stimuli-responsive behavior. These nanostructured gels can act as nano-reservoirs for controlled inhibitor release, facilitate self-healing at damaged sites, as well as reduce ion permeability by forming a dense, crosslinked network.

4.1. Nanoparticles

Nanoparticle incorporation into gel-based coatings has been presented as an effective strategy to enhance barrier performance and introduce active protection. Oroujzadeh et al. studied zirconium-based metal–organic gel (Zr-MOG) nanoparticles in epoxy matrices [86].

These nanogels have a high specific surface area of 455.7 m^2/g with an average pore diameter of 1.2 nm and pore sizes in the range of 1–5 nm. This high surface area can play a role in the adsorption mechanism for corrosion inhibition. Morphologically, FE-SEM analysis reveals aggregated nanostructures composed of 100–500 nm particles with smaller features below 100 nm, while DLS measurements indicate an average particle size of 89 nm. Their electrochemical analyses indicated the impact of pH. The healing efficiencies reached 472.7%, 287.8%, and 208.8% in acidic, neutral, and alkaline conditions, respectively, after 24 h immersion in 3.5% NaCl. The total impedance of optimized coatings reaches 259.69 $k\Omega \cdot cm^2$ within 5 h and remains around 135.69 $k\Omega \cdot cm^2$ after 24 h in neutral media. Controlled release studies show zirconium ion concentrations of only 18–39 ppb and organic species of 14.42–29.45 ppm over 48 h depending on pH. This highlighted slow degradation and sustained inhibitor delivery. The corrosion protection mechanism was studied and demonstrated that nanoparticles actively participate in both anodic and cathodic processes by forming $Zr(OH)_4$ precipitates and TPA-Fe complexes. Additionally, enhancing epoxy crosslinking and adhesion leads to a compact Zr-MOG protective film that blocks harsh ions such as Cl^-, H_3O^+, and OH^- penetration [86]. In short, nanoparticle-reinforced gel coatings provide a unique combination of nano-barrier effects, intelligent inhibitor release, and self-healing capability.

AZ31B Mg alloys were anodized under variable voltages at high pH. Then, an epoxy-alkyl silane sol–gel reinforced with SiO_2 nanoparticles was deposited on top of the optimized anodic layers. 1-Methylimidazole was added to the gel to promote a partial epoxy ring aperture. A quick deterioration of the oxide film with immersion time was evident, showing a reduction in the protection efficiency of 76.5% after 16 h immersion. Figure 4 illustrates the evolution of electrochemical impedance behavior of anodized and sol–gel sealed systems as a function of immersion time in a chloride environment. A clear decrease in impedance values at low frequencies was observed. For the anodized coating (100V2), the polarization resistance (Rp) decreases from 13,557 $\Omega \cdot cm^2$ to 884 $\Omega \cdot cm^2$ after 16 h of immersion. This fast decline indicates the limited long-term stability of porous anodic oxide layers. In contrast, the incorporation of gel coating enhances corrosion resistance. The epoxy-alkyl hybrid silica sol–gel (SGMI)_110 system maintains a high Rp value (14,903 $\Omega \cdot cm^2$ even after 72 h of immersion) [32]. Additionally, the SGMI_160 system exhibits lower resistance (1546 $\Omega \cdot cm^2$ after 72 h), which can suggest faster degradation. This difference can be attributed to the higher crosslinking density at elevated curing temperature. These results emphasize the critical role of both sealing treatment and curing conditions in controlling the long-term electrochemical stability of gel-Si NPs coatings.

Beyond traditional nanoparticles, two-dimensional nanosheet fillers such as hexagonal boron nitride (h-BN) illustrate how nano-structuring can alter the barrier performance of gel coatings as reported by Akbarzadeh et al. [87]. In gel-sealed plasma electrolytic oxidation (PEO) systems on AA2024, the incorporation of h-BN at 1000 and 2000 ppm was investigated for corrosion protection. Pristine h-BN without functional groups disrupts the gel network and reduces corrosion resistance. In contrast, oxidized and especially APTES-functionalized nanosheets enhance coating compactness and performance. Quantitatively, optimized coatings containing functionalized h-BN (PS-F2) exhibit outstanding electrochemical stability, with inner-layer resistance ($R_{mix,in}$) reaching 5.33×10^7 $\Omega \cdot cm^2$ after one week of immersion in 0.1 M NaCl. Additionally, poorly dispersed systems (PS-N_2) show degradation and an increase in effective capacitance up to 34.67 $nF \cdot cm^{-2}$, which indicates electrolyte penetration. For structural analysis, the degree of network condensation, such as the (Si-O-Si)/(Si-OH) ratio, increases from 1.86 in neat sol–gel to 2.42 in functionalized gels, which reflects enhanced crosslinking and densification [87]. Moreover, FE-SEM observations demonstrate effective pore sealing and homogeneous nanosheet dis-

tribution. Therefore, nanosheet-based fillers act as passive barriers and structural modifiers that improve the gel network.

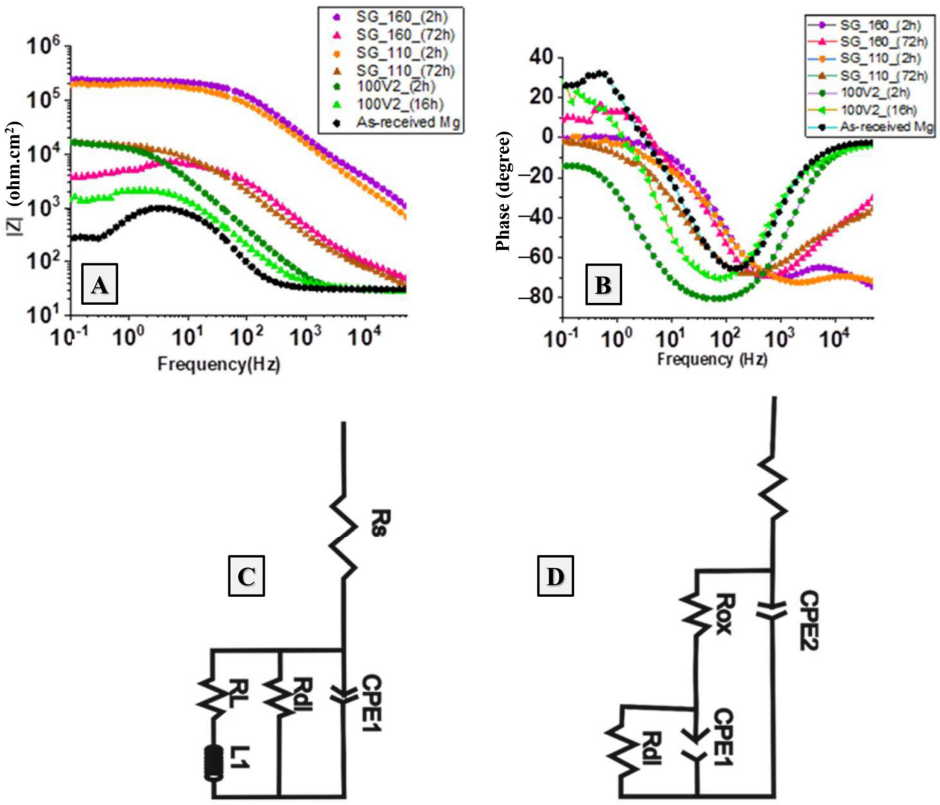


Figure 4. (**A**) Bode plots of impedance magnitude and (**B**) phase angle for the anodized coating (100V2), SG_160, SG_110, and as-received Mg alloy at different immersion times in 3.5 wt% NaCl solution. (**C**) Equivalent circuit for 100V2 after 16 h and SG_160 after 72 h of immersion, and (**D**) equivalent circuit for SG_110 after 72 h of immersion. Reproduced from Merino et al. [32] under CC BY 4.0 license.

4.2. CNT, Graphene, Nanodiamond

Carbon-based nanostructures such as carbon nanotubes (CNTs), graphene derivatives, and nanodiamonds have attracted considerable attention in gel coatings because of their high aspect ratio, mechanical strength, and impermeability to corrosive species [88–90]. Nanofillers act as physical barriers that elongate diffusion pathways as well as structural modifiers that enhance network densification, interfacial bonding, and coating. Their surface functionalization is critical, as it governs dispersion stability and interaction with the siloxane network. In addition, recent studies have begun to use computational tools such as artificial neural networks (ANNs) to better understand and predict the complex electrochemical behavior of such nanostructured coatings. The incorporation of oxidized multi-walled carbon nanotubes (O-MWCNTs) into silane gel coatings provides a clear image of how carbon nanostructures can impact corrosion protection, as reported by Akbarzadeh et al. [91]. By increasing the O-MWCNT content from 0.05 to 0.9%, a clear improvement in coating properties is found. FT-IR analysis reveals an increase in the Si-O-Si/O-H ratio from 2.22 to 9.02, which indicates a transition toward a more condensed siloxane structure. Cross-sectional SEM images show an increase in coating thickness from 1.59 ± 0.21 µm (neat silane) to 6.24 ± 0.35 µm at the highest CNT loading. For electrochemical evaluation, EIS results demonstrate a substantial increase in R_{ct} from 66.7 kΩ·cm^2 (neat coating, 24 h) to 359.5 kΩ·cm^2 for CNT coatings. Additionally, a rise in film resistance (R_f) to 286.5 kΩ·cm^2 confirmed enhancement in barrier properties. Moreover, low-frequency impedance values

increased from 4.73 to 5.81. Polarization measurements indicated a reduction in i_{corr} from 5.40 $\mu A \cdot cm^{-2}$ to 0.04 $\mu A \cdot cm^{-2}$. This value is an improvement of more than two orders of magnitude as well as a shift of corrosion potential toward more noble values. These enhancements are attributed to the dual role of O-MWCNTs (physically blocking pores and extending diffusion pathways) and chemically interacting with silanol groups (Si-O-C bonding) to reinforce the hybrid network. Additionally, the stability and predictability of such nanocomposites are demonstrated through ANN modeling and achieve high accuracy with $R^2 = 0.9879$ [91], which highlights the potential of incorporating carbon nano structuring with gel coatings.

Afsharimani et al. studied the effect of graphene nanosheets to improve gel coatings in corrosion inhibition [92]. In the GPTMS-TEOS-colloidal silica nanoparticles (GTS), the incorporation of silica nanoparticles increased coating thickness from 2.1–2.3 µm to 5.3–5.5 µm and surface roughness from 0.5 nm to 3.6 nm. For wettability, the contact angle values increased to 74° for GTS/GN-coatings. To evaluate the barrier performance in corrosion protection of silica-based coatings, Figure 5A presents the potentiodynamic polarization behavior of the bare AA2024 alloy compared with silica coatings with and without colloidal silica nanoparticles. The uncoated alloy demonstrates corrosion activity in chloride-containing environments. For the GT system, a reduction in i_{corr} is observed, which can reflect the formation of a partial barrier between the electrolyte and the metal surface. However, the most pronounced improvement is achieved when colloidal silica nanoparticles are incorporated (GTS system). In this case, the polarization curve shifts toward lower current densities and displays an extended passive region, which can be attributed to the increased structural compactness and thickness of the coating. Then, the influence of graphene nanosheets on corrosion protection was investigated through electrochemical polarization as shown in Figure 5B. The incorporation of chemically modified graphene nanosheets into the gel leads to an improvement in corrosion resistance. A shift in corrosion potential was seen. The polarization measurements show that the j_{corr} decreased from 3.0 ± 0.5 $\mu A \cdot cm^{-2}$ (bare AA2024) to 0.5 ± 0.1 $\mu A \cdot cm^{-2}$ (GT) and down to 0.03 ± 0.01 $\mu A \cdot cm^{-2}$ (GTS). The addition of chemically modified graphene nanosheets leads to a better reduction in j_{corr} to 0.002 ± 0.001 $\mu A \cdot cm^{-2}$. Additionally, there was a positive shift in corrosion potential from -0.48 ± 0.03 V to approximately -0.32 V. This superior performance can be attributed to the combined effects of enhanced crosslinking (Si-O-Si and Si-O-C bonding), pore filling by silica nanoparticles, and the high aspect ratio of graphene nanosheets. All these factors create a highly difficult diffusion pathway for corrosive species. Furthermore, the increase in hydrophobicity and surface roughness reduces water uptake [92]. In short, the combination of graphene nanosheets and silica nanostructures produces a dense, highly impermeable hybrid network.

In 2020, Li et al. studied a sol–gel layer filled with graphene oxide for corrosion protection of Ti6Al4V [93]. EIS reveals that the diffusion resistance (Warburg element) increases with GO incorporation. It was found at 1.60×10^6 $\Omega \cdot cm^2$ for the P/S-GO100 sample. The i_{corr} decreases from 1.17×10^{-7} $A \cdot cm^{-2}$ (P/S-GO0) to 1.88×10^{-8} $A \cdot cm^{-2}$ (P/S-GO100). Additionally, there is a positive shift in corrosion potential to 0.47 V. However, excessive GO addition (P/S-GO150) leads to performance deterioration, with i_{corr} around 2.85×10^{-8} $A \cdot cm^{-2}$ and a lower E_{corr} of 0.29 V. This can be due to agglomeration effects that disrupt coating uniformity and create defect pathways. The open circuit potential remains stable for 24 min in P/S-GO100, compared to only 14–18 min for lower or higher GO contents. This indicates that the corrosion protection mechanism is governed by the intrinsic impermeability of graphene oxide in addition to its dispersion state and interaction with the silane matrix [93].

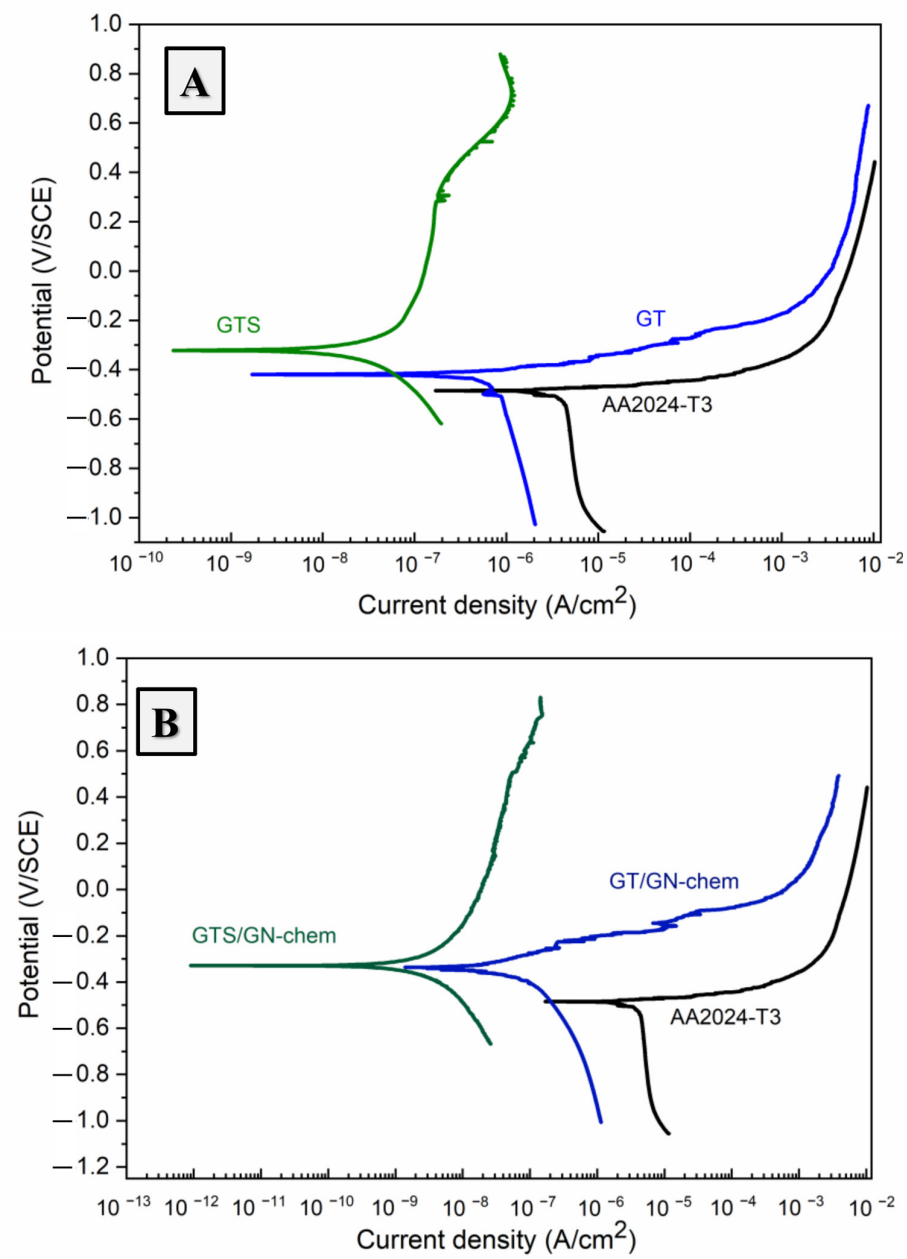


Figure 5. (**A**) Potentiodynamic polarization curves of bare AA2024-T3 alloy and coated with gel without and with colloidal SiO_2 NPs denoted as GT and GTS, respectively. (**B**) Potentiodynamic polarization curves of bare AA2024-T3 and coated with gel including graphene nanosheets. Reproduced from Afsharimani et al. (2020) [92] under CC BY license.

The incorporation of hydroxylated nanodiamonds (HNDs) modified the resistive and capacitive responses of the gel coating in corrosion inhibition application [94]. The impedance analysis showed that the polarization resistance (R_p) of the optimized coating (0.01% HND) reached 111.01 kΩ·cm^2 after 60 min immersion and only 12.09 kΩ·cm^2 for the neat gel coating, without HND. This represented nearly a ninefold enhancement in corrosion resistance. Additionally, capacitance parameters (Q_f) increased with immersion time, which reflects electrolyte uptake and the lowest Q_f values observed for the 0.01% HND coating. This indicates minimized water diffusion and a more compact structure. Polarization measurements were used to check the J_{corr}, and it decreased from 2.202 μA·cm^{-2} (0%) to 0.476 μA·cm^{-2} at 0.01% HND. This was observed along with a positive shift in corrosion potential from −1.519 V to −1.335 V. Increasing the nanoparticle content to 0.02 and 0.05% gave higher J_{corr} values around 0.745 and 1.884 μA·cm^{-2}, respectively. This means higher

loading from HND reduced protection efficiency, which can be due to partial agglomeration and defect formation. Morphological observations after corrosion displayed no visible degradation for 0.01%–0.02% coatings, while clear delamination occured at 0.05% [94]. This emphasizes that optimal nanoparticle loading governs initial barrier properties and electrochemical stability under aggressive conditions.

4.3. MOFs and Advanced Fillers

Metal–organic frameworks (MOFs) have recently emerged as a promising class of advanced fillers in gel-based coatings [95–97]. This can be due to a unique combination of high porosity and capability to act as smart nanocontainers for corrosion inhibitors [81,98,99]. Chen et al. studied the development of a benzotriazole (BTA)@ZIF-8/sol–gel composite which was prepared via a facile one-step in situ growth method [82]. The incorporation of BTA promotes the formation of a compact ZIF-8 layer and provides active corrosion inhibition because of interaction with Cu-rich intermetallic phases. Quantitatively, the coating with 2.6 μm thickness exhibits long-term performance with a low-frequency impedance of 10^6 Ω·cm^2 after 30 days of immersion in 3.5% NaCl. Electrochemical analysis confirmed that the degradation of sol–gel coatings occur within 3–14 days, whereas the presence of the MOF layer delays it to 30 days. This indicates a promising retardation of electrolyte penetration and interfacial reactions. Moreover, the high-frequency phase angle remains around $-50°$ after 30 days for MOF coatings, and it was found at $-10°$ for unmodified gel. The ideal dielectric coating should have a phase angle of $-90°$ [100], but practical coatings rarely achieve this value because of surface roughness, heterogeneity, finite ionic conductivity, and water uptake. Therefore, the observed high-frequency phase angle of approximately $-50°$ should not be interpreted as ideal capacitive behavior but rather as evidence of a mixed capacitive–resistive response characteristic of real coating systems. This behavior is represented by a constant phase element (CPE) in equivalent circuit analysis. When considered together with the high low-frequency impedance modulus and stable electrochemical response during immersion, the $-50°$ phase angle indicates that the MOF coating maintains an effective barrier against electrolyte penetration while suppressing charge-transfer processes. The enhanced performance after MOF modification can be attributed to a dual protection mechanism. The MOF layer acts as a physical barrier and enables pH-triggered release of inhibitors (BTA and 2MI). This smart release is controlled by local pH gradients during corrosion. Additionally, the MOF particles exhibit 8.1% inhibitor loading capacity and interfacial adhesion exceeding 20 MPa. In short, MOF fillers can transform gel coatings from passive barriers into self-responsive inhibitors for long-term corrosion protection [82].

Another study of MOF-based fillers was investigated by Mohammadpour et al., including the incorporation of 2-aminobenzothiazol (2-ABT)-Cu-1,3,5-tricarboxylate (Cu-BTC MOF) particles into electro-assisted silica sol–gel coatings [101]. The Cu-BTC framework exhibits a high inhibitor loading capacity of around 10.7 mg per 100 mg MOF. It achieved 40% controlled release within 24 h. The J_{corr} decreased from 19.62 μA·cm^{-2} (bare Ni-Fe alloy) to 10.37 μA·cm^{-2} (pure silica coating) and went down to 2.10 μA·cm^{-2} for the optimized silica/MOF3 coating. The corrosion potential changed from -544.5 mV to -269.6 mV. Additionally, an increase in polarization resistance (R_p) was seen from 1.57 kΩ·cm^2 to 11.69 kΩ·cm^2 and a reduction in coating porosity to 0.3%. The inhibition efficiency reached 98.87% for the silica/MOF3 system at optimal concentration (0.037 g/L). After inhibitor optimization, the Rp increased to 74.6 kΩ·cm^2. This behavior can be attributed to the dual-function mechanism of MOFs: (i) improving coating compactness and reducing electrolyte pathways, as well as (ii) enabling time-dependent release of active molecules such as 2-aminobenzothiazole, which adsorbed on the metal surface via heteroatoms (N, S) and

π-electrons [101]. In short, MOF-based fillers provide a synergistic combination of passive barrier and active self-healing protection.

5. Functional Gel Coatings

Beyond passive barrier protection, modern gel-based coatings are designed and engineered to have active and adaptive functionalities that can respond to environmental stimuli and damage environments [102–104]. These systems represent a shift from traditional coatings toward smart protective coatings, which are capable of responding to abnormal corrosion processes in real time. Functional gel coatings can repair damage, regulate ion diffusion, and provide early-stage corrosion inhibition [105–108]. Among the reported functional gels, self-healing, pH-responsive, and sensing coatings are promising, as they address the critical limitations of traditional coatings [27,109].

5.1. Self-Healing Coatings

Self-healing gels can be considered as one of the most effective strategies to extend the life of metallic substrates by restoring protective functionality after mechanical or chemical damage [8,110,111]. Xu et al. introduced the integration of MOF-based nanocontainers within sol–gel by designing a ZnO/ZIF-8@2-mercaptobenzothiazole (MBT)/sol–gel composite coating [105]. In this gel, the self-healing characteristic arises from the synergistic interaction between encapsulated inhibitors and responsive components. ZIF-8 acts as both a carrier for MBT and 2-methylimidazole (2-MI) source. Upon coating damage and electrolyte penetration, these species are released and adsorb onto exposed metallic regions to form a protective film. Quantitative electrochemical and surface potential analyses confirm this self-repair capability. Scanning Kelvin probe measurements show that the potential difference (ΔE) between damaged and intact regions decreases from −714 mV to 214 mV after 6 h. This rapid equilibration indicates effective re-passivation of the damaged area. Additionally, cyclic EIS reveals partial recovery of impedance values during exposure. At the molecular level, the self-healing mechanism is controlled by co-adsorption and synergistic inhibition. The combined presence of MBT and 2-MI leads to the formation of a dense adsorption layer on the alloy surface. This synergy is supported by a calculated synergistic factor (SF = 1.15). Density functional theory calculations further reveal that co-adsorption enhances binding strength, with adsorption energy improving to −2.092 eV, compared to −1.359 eV and −0.872 eV for MBT and 2-MI, respectively. Therefore, the sol–gel top layer can serve as a physical barrier in addition to regulating the release kinetics of inhibitors [105]. This hierarchical design illustrates the next generation of self-healing coatings, where repair processes are localized and tightly coupled to corrosion activity.

In addition to MOF incorporation, recent advances have highlighted the potential of bio-based gel microspheres for sustainable gel coatings [112–114]. Liu et al. introduced the incorporation of tea polyphenol@graphene oxide@polyvinyl alcohol (TGPG) hydrogel microspheres into a polyaspartic ester (PAE) gel through a one-step blend–cryogenic–in situ crosslinking strategy. This method presented uniformly dispersed microspheres that were chemically combined in the gel network. The coating exhibited promising corrosion resistance. The low-frequency impedance modules increased from 9.3×10^8 to 5×10^9 Ω·cm^2. The performance was stable after 28 days of immersion as well as 1000 h salt spray exposure. The self-healing mechanism is governed by multiple synergistic effects. Upon damage, water penetration induces microsphere swelling (1.2–1.3 times), facilitating crack filling, and the controlled release of tea polyphenols promotes metal–polyphenol chelation. This chelation forms a protective passivation layer. Additionally, the photothermal effect of graphene oxide increases the local temperature to 46 °C, which exceeds the glass transition temperature of the matrix (43–44 °C). So, the coating restores

its protective performance, with impedance recovering to 1×10^9 Ω·cm^2 and stabilizing around 8×10^9 Ω·cm^2 after healing [110].

The strategy for self-healing coatings was reported by inhibitor-loaded plasma electrolytic oxidation (PEO) combined with sol–gel sealing [115]. In this method, corrosion inhibitors such as benzotriazole (BTA) and 8-hydroxyquinoline (8-HQ) were introduced into PEO pores at concentrations ranging from 1 to 20 g/L with a sol–gel top layer to enhance barrier properties. Electrochemical analysis revealed a synergistic effect at an optimized 8-HQ/BTA ratio of 7:3 to achieve an inhibition efficiency of 93% after 72 h in 0.1 M NaCl solution. Structurally, the PEO coating has a thickness of about 12.8–13.4 μm, with pore sizes in the range of 1–10 μm. Long-term impedance measurements demonstrated the effectiveness of this gel. In the case of the optimized gel, low-frequency impedance values exceeded 10^8 Ω·cm^2 after two weeks. The intermediate inhibitor concentration of 5 g/L provides the best balance between pore filling and sol–gel adhesion. The self-healing mechanism arises from the triggered release of inhibitors in the case of electrolyte penetration. BTA passivates Cu-rich intermetallic sites while 8-HQ forms chelating complexes to suppress both anodic and cathodic reactions [115].

Another direction in self-healing coatings involves ethyl cellulose-based supramolecular gel enriched with functional inhibitors or responsive nanoparticles. Lin et al. introduced coatings pre-loaded with high concentrations of imidazoline inhibitors (up to 25%) [26]. Electrochemical measurements indicated that the C17 inhibitor achieved up to 91% inhibition efficiency at 10×10^{-4} mol/L in 3.5% NaCl. The overall coating performance improved with increasing chain length due to better hydrophobic barrier formation. However, coatings containing 25% C11 exhibit the most effective self-healing under damaged conditions, because the higher release rate facilitates rapid formation of a protective adsorption film. This is reflected in the corrosion potential, which shifted from −621 mV to −451 mV (vs. SCE) for coatings without inhibitor and from −557 mV to −493 mV for the inhibitor system after 7 days. In another study, supramolecular gel coatings incorporating 10% Fe_3O_4 nanoparticles introduce an externally triggered healing mechanism based on electromagnetic heating [116]. Under an alternating magnetic field, these coatings can reach healing temperatures near 80 °C using a rate of about 1.64 °C/s, which enables defect closure within 58 s. The reversible nature of hydrogen bonding and van der Waals interactions allow the coating to undergo repeated healing cycles (up to 10 cycles). Therefore, combining highly loaded responsive inhibitors with supramolecular networks extends coating life by enabling both autonomous and on-demand self-healing responses.

5.2. pH-Responsive Systems

pH-responsive gel coatings represent a key type of smart protective system in which corrosion-triggered local pH variations occur [117–119]. These pH-responsive gel systems exploit the fact that anodic and cathodic reactions during corrosion generate localized acidic or alkaline environments. These generated protons can be used to activate gel swelling, nanocontainer opening, or chemical release processes. In 2023, MOF-based pH-responsive nanocontainers were introduced by Huang et al. [25]. This was based upon BTA-ZIF-8 assembled on hydroxylated hexagonal boron nitride (BN-OH) within sol–gel coatings. These hybrid systems combine active inhibition and passive barrier effects. ZIF-8 frameworks provide pH-triggered release of encapsulated BTA under both acidic and alkaline conditions, while BN nanosheets introduce a “labyrinth effect” that limits the diffusion of aggressive species. So, coatings incorporating these nanocontainers exhibit an improvement in long-term corrosion resistance, with low-frequency impedance values reaching 2×10^8 Ω·cm^2 after 28 days of immersion. These values are three orders of magnitude higher than those of the unmodified sol–gel coating. Moreover, scratched coatings show increasing impedance

over time, which confirms effective self-healing through on-demand inhibitor release and re-passivation of exposed sites [25]. In 2024, Samadianfard et al. reported a pH-responsive gel through functional nanocarriers embedded in sol–gel matrices, such as losartan-loaded graphitic carbon nitride (g-C_3N_4@LP) nanoplates [120]. These layered nanostructures (with hydrodynamic sizes of 803 nm) enable controlled inhibitor storage. The incorporation of 100 ppm of g-C_3N_4@LP leads to uniform, crack-free coatings with reduced surface roughness (1.60 μm instead of 1.77 μm) and significantly enhanced corrosion resistance. Electrochemical measurements show that the polarization resistance reaches 1.782 MΩ·cm^2 after 120 h immersion. It represents an increase of more than 18 times compared to the unmodified coating. The inhibitor release is strongly pH-dependent, reaching a maximum in alkaline conditions (pH 10–12) and stabilizing after 1 h, which confirms rapid response to corrosion initiation while preventing excessive leaching [120]. In 2025, Fang et al. introduced the incorporation of tannic acid (TA) and benzotriazole (BTA) to form tannic acid @ Benzotriazole @ Poly(hydroxypropyl acrylate-triethoxyvinylsilane-acrylic acid)/polyethyl enimide (TBP) gel embedded in epoxy coatings [121]. Upon water uptake, the gel expands and fills microdefects, while pH-mobility release of inhibitors leads to the formation of protective adsorption films and iron-tannate complexes on the metal surface. This dual mechanism improves long-term performance, and the impedance values were found to be as high as 2.36 × 10^7 Ω·cm^2 after 181 days of immersion. The neat epoxy coating decreased to 6.86 × 10^4 Ω·cm^2. Additionally, adhesion properties were improved and increased by 18.2% in dry adhesion and 74.7% in wet adhesion [121]. This highlights the promising interfacial compatibility introduced by siloxane bonding within the gel structure. In short, pH-responsive gel coatings can be designed across multiple length scales from polymeric gels to nanostructured carriers and MOF-based architectures for achieving corrosion-triggered functionality. The combination of stimuli-responsive swelling, controlled inhibitor delivery, and enhanced barrier properties provides a promising pathway toward intelligent coatings capable of adapting dynamically to aggressive environments.

5.3. Sensing Coatings

In addition to protective and responsive functions, gel-based coatings are designed as integrated sensing substrates for real-time corrosion monitoring toward intelligent coating systems [122]. A recent advancement in this direction is the development of a flexible electrochemical sensing device incorporating a poly(vinyl alcohol) (PVA) gel electrolyte. Unlike traditional electrolytes, the PVA gel provides excellent adhesion [123–125], shape conformity, and electrolyte retention. The gel electrolyte exhibits sufficient ionic conductivity at 11.44 mS·cm^{-1} for 0.1 M KCl and 2.00 mS·cm^{-1} for 0.01 M KCl. Electrochemical performance evaluation demonstrates that the gel-enabled device can reproduce corrosion inhibition. For example, anodic polarization measurements of copper show an immersion potential near −10 mV, and corrosion current increases across flat and curved geometries. Furthermore, the device enables quantitative analysis of corrosion products through cathodic reduction measurements. A clear reduction was observed at −0.8 V (Cu_2O and Ag_2S reduction) and −1.2 V (hydrogen evolution). Using these values, corrosion film thicknesses can be determined and found at 2.13 μm (sticker device) vs. 2.19 μm (conventional system) for Cu_2O, and 723 nm (horizontal) and 694 nm (curved) compared to 689 nm for Ag_2S. The sensing capability is supported by the stability of the integrated reference electrode, which maintains a consistent potential over extended periods (up to 48 h) under both liquid and gel conditions. Also, the device shows robustness against mechanical deformation. This combination of mechanical flexibility, electrochemical accuracy, and environmental adaptability enables continuous monitoring of corrosion processes and corrosion product

evolution [122]. In short, gel-based sensing coatings illustrate the transition from passive protection to multifunctional gels that integrate protection and diagnostics.

6. Gel-Based Coatings in Concrete and Civil Applications

The application of gel-based coatings in civil applications has received much attention to enhance the durability of reinforced structures [29,126–128]. These structures can be exposed to aggressive environments such as chlorides [129], moisture [130], and pH change [131]. In reinforced concrete, the corrosion of steel rebars is one of the primary causes of structural degradation because it leads to cracking, spalling, and loss of mechanical properties. Gel-derived coatings can offer unique advantages in this problem, such as better adhesion to metallic substrates, and resistance to alkaline concrete pore environments. By combining barrier protection with mechanical enhancements, these coatings serve as effective interfaces that retard ion transport and delay corrosion initiation.

6.1. Rebar Protection

Gel-based coatings were studied to protect steel reinforcement within concrete. Xu et al. introduced the use of polydimethylsiloxane (PDMS)/SiO_2 hybrid gel coatings, which were synthesized via a base-catalyzed sol–gel process with varying silica contents (0%–20%) [132]. The incorporation of SiO_2 into the PDMS matrix introduces a clear synergistic effect, where mechanical properties such as Young's modulus and yield strength increase. This indicates improved stiffness and structural integrity. From electrochemical analyses, EIS and polarization studies reveal an enhancement in corrosion resistance compared to uncoated steel in concrete pore solutions. The coating containing 15% SiO_2 exhibits optimal performance and achieves an inhibition efficiency of 95.8%. This can be attributed to dense hybrid networks that effectively restrict the penetration of aggressive ions. Surface analysis confirmed the smooth, crack-free morphology after 24 h immersion, but uncoated rebars show signs of corrosion product formation and surface degradation [132]. Similarly, crack-free gel coatings based on polyvinyl butyral (PVB)/silica nanocomposites provide an effective route for rebar protection in chloride-containing concrete environments, as reported by Meng Zhang [133]. Young's modulus increased from 36.3 MPa for pure PVB to 94.5 MPa because of the incorporation of 15% silica. This reflects an enhanced rigidity and resistance to mechanical damage. Electrochemical studies indicate that the optimal corrosion resistance is achieved at 10% silica loading, and the coating delivers an inhibition efficiency of 89.3% after 2 days of exposure in simulated concrete pore solution [133]. The observed performance can be due to the formation of a uniform, defect-free barrier layer, which minimizes electrolyte penetration and delays the onset of corrosion reactions. In short, the effectiveness of gel-based rebar coatings strongly depends on composition optimization and microstructural control. The incorporation of silica within polymeric gel matrices enhances mechanical durability as well as improves resistance to corrosion. Such hybrid gel coatings offer a promising pathway toward crack-resistant protective systems for reinforced concrete structures.

6.2. Crack Repair Gels

Gel-based crack repair systems are multifunctional solutions that can restore the physical properties of concrete. Among the reported gels, bio-inspired gels based on microbially induced calcium carbonate precipitation (MICP) have been studied by Fan et al. [29]. This bio-gel composed of bacterial solution and calcium alginate acts as both a self-mineralizing filler and a chloride-binding medium. The gel demonstrates strong adsorption capacity for aggressive ions. The capacity reached 118.3 mg/g, which is about 31.6% higher than that of traditional alginate gels. This enhanced ion-binding capability retards chloride

transport toward the steel surface. From structural analysis, cracks with widths up to 1 mm can be completely sealed within 15 min. Electrochemical measurements highlight the protective role of the bio-gel because the corrosion current of embedded steel decreases to around 2.88×10^{-6} mA·cm^{-2}. In reinforced concrete specimens, the corrosion reduction reached 88.7%, which confirms the effectiveness of the gel in real structural environments. The mechanism is attributed to a combination of physical blocking, chloride adsorption, and pore densification by mineral deposition [29]. The long-term evolution of corrosion behavior in reinforced concrete was studied. The Rp value of untreated cracked concrete (CG) decreased from 555 to 433 Ω·cm^2 over 14 days. In contrast, specimens repaired with calcium alginate gel (CA) and bio-gel (CAB) exhibit higher initial Rp values of 3109 and 4890 Ω·cm^2, which remain comparatively elevated after 14 days (1799 and 3847 Ω·cm^2, respectively). A similar trend is observed where the corrosion current values provide direct insight into corrosion kinetics. The untreated i_{corr} increased from 0.6425 to 0.8244 μA·cm^{-2} over time. In comparison, lower values are recorded for CA (0.073 to 0.0928 μA·cm^{-2}) and CAB (0.1151 to 0.1988 μA·cm^{-2}). The bio-gel system achieved an overall corrosion reduction of 88.7% relative to the untreated case. This behavior confirmed that the bio-gel seals cracks and slows down steel corrosion through a combination of chloride binding, oxygen barrier effects, and pore densification via calcium carbonate precipitation [29]. In parallel, synthetic alkaline hydrogels provide an alternative strategy by combining crack sealing with chemical reconditioning of the concrete environment. Hydrogels based on diallyldimethylammonium hydroxide, modified with acrylic acid, function as "3-in-1" systems [134]. They are able to seal cracks, restore alkalinity, and re-passivate steel reinforcement. Their performance is driven by a zwitterionic network structure, which generates significant swelling pressure upon water uptake. This is demonstrated by leakage tests, where no water penetration is observed for more than 28 days. Simultaneously, the high alkalinity of the gel promotes re-passivation of steel. To conclude, crack repair gels have evolved into integrated protective systems that combine rapid crack sealing with long-term corrosion control.

7. Bio-Based and Eco-Friendly Gel Coatings

Currently, replacing toxic corrosion inhibitors with bio-safe and eco-friendly inhibitors is an interesting point [135]. The bio-based gel coatings can be considered as sustainable alternatives [110,136–138]. These systems use naturally derived or biologically safe components to introduce functionality and electrochemical stability of metal substrates. Unlike traditional coatings, bio-based gels can be designed to interact dynamically with the surrounding environment to offer adaptive responses to microbial activity, pH change, and moisture attack. This class of gel coatings integrates principles from materials science, microbiology, and green chemistry to reduce ecological impact with corrosion protection performance.

7.1. Bio-Gels for Corrosion Protection

Bio-gel coatings represent a novel strategy to address microbially influenced corrosion (MIC). In these aqueous systems, biofilm formation plays a critical role in degradation. An example involves the integration of *Bacillus clausii* spores and biosurfactants into silica-based sol–gel [139]. A partial reduction in spore viability within the gel network demonstrates approximately 20.8% survival, corresponding to 1.71×10^6 CFU/mL. The presence of bio-components enhanced surface hydrophobicity. The contact angles increased from 60.6° (bare steel) to 93.25° in spore coatings and 83.22° in biosurfactant-modified systems. The role of hydrophobicity can play a promising function in limiting water penetration and microbial adhesion. Biofilm formation decreased, as observed via a reduced bacterial population of 2.23×10^5 CFU/mL at the maturation stage for biosurfactant-containing

coatings. Additionally, a delay in biofilm development of up to 12 days was found in spore-functionalized systems. Electrochemical performance indicated the protective role of bio-gels: after prolonged exposure (180 days), biosurfactant-loaded coatings maintain a remarkably low corrosion current density (i_{corr} = 0.51 $\mu A/cm^2$) and high impedance values (10^4 $\Omega \cdot cm^2$). Surface analyses revealed smoother and more uniform morphologies with iron exposure (0.12% Fe) [139]. Mechanistically, these bio-gel systems worked through a combination of physical barrier effects, antimicrobial activity, and inhibition of biofilm-mediated electrochemical processes.

A complementary perspective on bio-gel systems is introduced by Ghuzali et al. through the preparation of plant extract-functionalized sol–gel coatings. Clitoria ternatea extract-incorporated silica coatings demonstrate how bio-derived compounds can actively enhance electrochemical performance. The incorporation of ethanol-extracted bioactive molecules at an optimal concentration of 75 ppm leads to a decrease in corrosion current density from 618 $\mu A \cdot cm^{-2}$ (bare steel) to 64.2 $\mu A \cdot cm^{-2}$. This corresponds to an inhibition efficiency of 89.6%, while water-based extracts achieve 85.6% efficiency under a similar environment [140]. EIS showed an increase in charge transfer resistance up to 488 $\Omega \cdot cm^2$ and inhibition efficiencies exceeding 83%, indicating the formation of a more resistive interfacial layer. These improvements are linked to the antioxidant-rich composition of the extract, such as flavonoids like quercetin. These biomolecules can promote adsorption onto the metal surface and facilitate the formation of protective Fe-O-Si bonds. Morphologically, SEM images revealed smoother and more homogeneous surfaces for bio-gel-coated substrates, while EDX analysis showed reduced oxygen content and higher iron retention (92% Fe for extract-modified coatings versus 68.67% in unprotected samples) [140]. From a mechanistic point of view, these bio-gel coatings act through a synergistic combination of barrier enhancement, antioxidant activity, and interfacial chemical bonding.

7.2. Natural Extracts for Corrosion Protection

For natural extracts, the incorporation of *Clitoria ternatea* [141] and caffeine [142] as a green inhibitor within TEOS-APTES hybrid sol–gel provides an example of how small bioactive molecules can modulate both electrochemical behavior and surface properties of protective coatings. For the caffeine study, increasing caffeine concentration from 25 to 100 ppm enhanced corrosion resistance, with charge transfer resistance rising from 2441.65 $\Omega \cdot cm^2$ to 6218.02 $\Omega \cdot cm^2$ and an inhibition efficiency of 84.22%. This improvement is accompanied by a marked decrease in corrosion current density from 6.3096 $\mu A \cdot cm^{-2}$ (bare steel) to 0.7079 $\mu A \cdot cm^{-2}$ at 100 ppm, corresponding to a high inhibition efficiency of 88.79%, confirming a substantial suppression of electrochemical activity at the metal interface (page 7). Additionally, electrochemical noise analysis reveals an increase in noise resistance from 0.23 $k\Omega \cdot cm^2$ to 1.83 $k\Omega \cdot cm^2$, further evidencing enhanced barrier performance and reduced corrosion fluctuations (page 9). Surface characterization supports these electrochemical trends: SEM images show a transition from rough, pitted morphologies in uncoated samples to relatively smooth and defect-minimized surfaces upon caffeine incorporation, while EDX data indicates improved iron retention (85.44 wt.% Fe) and reduced chloride penetration (0.12 wt.% Cl) compared to untreated substrates (page 10). Moreover, wettability measurements highlight a shift toward hydrophobic behavior, with water contact angles increasing from 59.74° to 96.41°, implying reduced water affinity and improved coating integrity (page 11) [142]. Mechanistically, these enhancements are attributed to the adsorption of caffeine molecules via electron-rich O and N atoms, promoting the formation of stable interfacial bonds and a denser siloxane network, ultimately yielding a mixed-type inhibition effect that simultaneously retards both anodic and cathodic reactions.

Beyond *Clitoria ternatea* extract and caffeine, some plant-derived natural products have recently been incorporated into gel coatings as environmentally friendly corrosion inhibitors. Extracts obtained from green tea [110], henna (*Lawsonia inermis*) [143], neem (*Azadirachta indica*) [144,145], and other botanical sources [146] are rich in functional groups, which possess abundant hydroxyl, carbonyl, and aromatic functional groups able to interact with metallic substrates. These phytochemicals can play a promising role in protection by being adsorbed at the surface of metal. This adsorbed layer forms a fixed metal–organic layer, which can decrease the reaction between metal and reactive oxygen species. Furthermore, their incorporation into gel systems enables controlled release of active corrosion inhibitors. These findings demonstrate that plant extracts represent an expanding type of sustainable additives for gel corrosion-protective coatings.

Tea polyphenols have been studied after incorporation into graphene oxide/poly(vinyl alcohol) (GO/PVA) hydrogel microspheres within a polyaspartic ester (PAE) coating to produce an intelligent self-healing anticorrosion system [110]. The phenolic hydroxyl groups of tea polyphenols give a dense hydrogen-bonding layer with PVA and GO, while their catechol part dynamically chelates Fe^{2+}/Fe^{3+} ions released during corrosion to generate protective passivation layers. Simultaneously, graphene oxide nanosheets support the hydrogel to provide a physical barrier against harsh ions. The composite coating provides long-term protection with an impedance above 10^9 $\Omega \cdot cm^2$ after self-healing and prolonged immersion. This demonstrates the synergistic contribution of natural polyphenol gel matrices toward intelligent protective coatings. Similarly, plant-derived extracts have been successfully incorporated into hybrid sol–gel coatings for biomedical metallic implants. Lawsonia inermis (henna) extract has been introduced into vinyltrimethoxysilane (VTMS)-based hybrid sol–gel coatings deposited on stainless steel 316L [143]. The hydroxyl- and carbonyl-containing phytochemicals in henna interact with the siloxane network without disrupting the gel structure and preserve promising coating adhesion as well as enhance corrosion resistance in simulated body fluid. The optimized coating (0.05 wt% henna extract) achieved protection efficiencies exceeding 90%. This result indicates that plant-derived extracts can improve corrosion resistance and adhesion, which makes them promising functional additives for protective coatings in orthopedic and dental implant applications. Neem (Azadirachta indica) has also been investigated as an attractive renewable source of green corrosion inhibitors for gel and polymer-based coating systems [144,145]. Encapsulated crude neem leaf extracts have been incorporated into epoxy coatings to provide active corrosion protection through a controlled release mechanism. Upon coating damage, the released phytochemicals adsorb onto the exposed aluminum surface and promote the formation of protective organic films. In alkaline chloride media, the encapsulated neem extract exhibited an extrinsic self-healing effect, while X-ray photoelectron spectroscopy confirmed the formation of corrosion-resistant surface species generated by the interaction between neem-derived compounds and the metallic substrate. In addition to leaf extracts, neem seed oil has been utilized as a renewable precursor for alkyd resin synthesis. Epoxy-modified neem oil alkyd coatings exhibited excellent curing behavior, enhanced hydrophobicity, improved thermal stability, and durable corrosion protection for steel substrates. This highlights the versatility of neem-derived products as sustainable alternatives to conventional coating materials.

7.3. Sustainable Coatings for Corrosion Protection

In the context of eco-friendly corrosion protection strategies, Domínguez-Martínez et al. investigated eco-friendly sol–gel coatings on AZ61 magnesium alloy [135]. The study highlights the role of naturally derived and low-toxicity compounds, such as L-cysteine, N-acetyl-cysteine, curcumin, and methylene blue, in coating performance. The macroscopic

corrosion behavior of these systems is illustrated in Figure 6, which presents photographic images of coated and uncoated samples before and after 14 days of immersion in NaCl solution. As shown in Figure 6, all samples exhibit some degree of surface degradation. This was evidenced by the formation of white corrosion products. However, significant differences in performance were observed depending on the type of incorporated inhibitor. The uncoated alloy had severe corrosion. In contrast, the presence of eco-friendly gel provides partial protection depending on inhibitor chemistry. Coating containing L-cysteine and N-acetyl-cysteine demonstrates improved surface preservation. On the other hand, the methylene blue-based coating exhibits pronounced degradation, indicating poor coating stability and adhesion under prolonged exposure. This behavior suggests that not all environmental additives are effective and that molecular structure can play a role in determining corrosion protection efficiency.

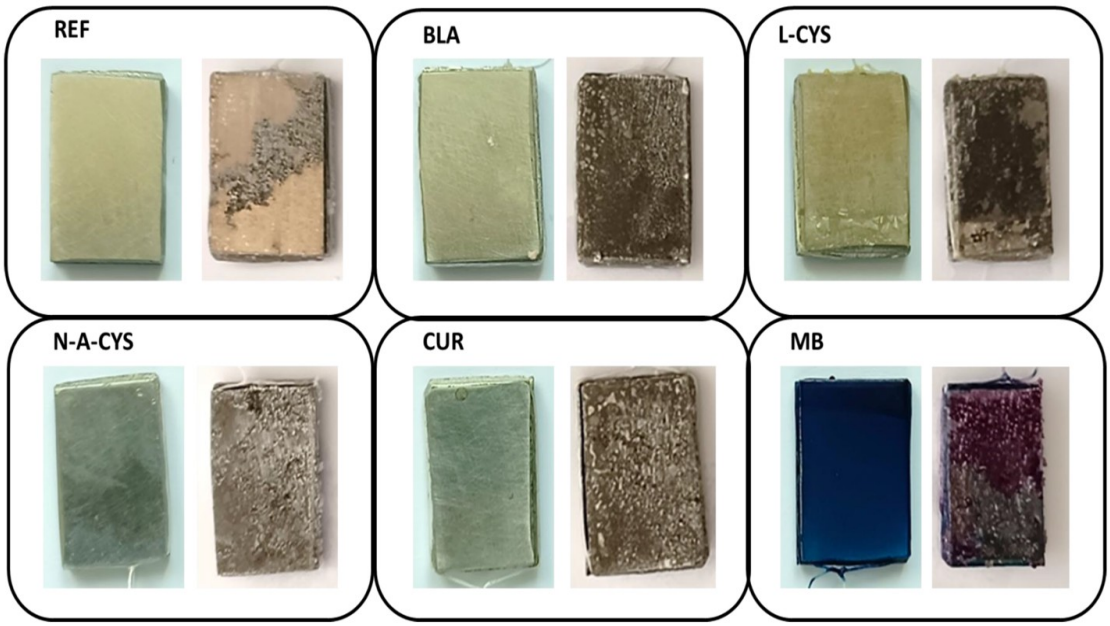


Figure 6. Photographic images of uncoated and gel-coated AZ61 magnesium alloy incorporating different eco-friendly organic inhibitors (L-cysteine, N-acetyl-cysteine, curcumin, and methylene blue) before and after 14 days of immersion in NaCl solution. Reproduced from Domínguez-Martínez et al. [135] under CC BY 4.0 license.

A particularly promising direction within sustainable gel-based coatings is the utilization of lignin as a bio-derived crosslinking component in hybrid sol–gel systems. It can offer both environmental and functional advantages. The incorporation of 3% modified lignin dissolved in a natural deep eutectic solvent (NADES) into organosilane/zirconium-based sol–gel formulations enables the fabrication of corrosion-resistant coatings on Al2024 substrates with significantly improved processing and performance characteristics. Notably, lignin addition enhances formulation stability by increasing viscosity, thereby improving shelf life, while simultaneously enabling room temperature curing, in contrast to conventional thermally cured systems. FTIR analysis confirms that coatings cured at ambient conditions exhibit a crosslinking density comparable to heat-cured analogs, indicating that lignin actively participates in network formation rather than acting as a passive filler. Morphologically, the resulting coatings are described as homogeneous, defect-free, and hydrophobic, attributes that are critical for effective barrier protection. From an electrochemical standpoint, the 3 wt.% lignin-containing coatings demonstrate superior corrosion resistance, even though they are thinner than lignin-free counterparts, highlighting the efficiency of the lignin-induced network in limiting electrolyte penetration and interfacial

degradation. This improved performance is attributed to the synergistic effect of dense hybrid crosslinking and the intrinsic aromatic structure of lignin, which enhances barrier properties and interfacial adhesion [147]. Overall, these findings emphasize that lignin-based hybrid gels not only reduce reliance on fossil-derived components but also enable energy-efficient processing routes, positioning them as a viable class of next-generation eco-friendly coatings for corrosion protection.

8. Comparative Analysis of Gel-Based Corrosion Protection Systems

The increase in the reported publications (Figure 1) reflects the evolution of gels corrosion protection technologies. Firstly, it focused on conventional sol–gel barrier coatings. Then, the studies moved to multifunctional gels. These gels are able to provide corrosion protection, self-healing, crack sealing, corrosion sensing, and environmentally sustainable performance. Significant technological advances have substantially enhanced coating durability, barrier properties, and long-term electrochemical stability. The recent gel coatings included the incorporation of nanomaterials, MOFs, bio-inspired additives, plant-derived corrosion inhibitors, and hybrid organic–inorganic networks. Furthermore, increasing environmental regulations have accelerated the replacement of toxic coatings with green and sustainable gel-based alternatives. These technological developments have collectively driven the rapid expansion of research in this field. The quantitative results reported throughout the recent literature about advanced gels for corrosion protection applications are organized in Table 2. It provides a clearer comparison of how different gels perform under various conditions. Despite differences in substrates, electrolytes, and testing environment, some consistent trends can be observed. Effective gel coatings have inorganic networks and interfacial bonding, such as hybrid sol–gel and ORMOSIL gels with high impedance values and low corrosion current densities. This can indicate effective barrier properties and long-term stability. The incorporation of nanoparticles such as carbon nanotubes, nanodiamonds, and boron nitride enhances performance by improving coating compactness and creating more tortuous pathways for corrosive protection. However, the literature reports show that this improvement is highly dependent on proper loading levels. Excessive filler content can introduce defects and reduce protection efficiency. More advanced systems, such as MOF-based, pH-responsive, and supramolecular gels, have an additional level of functionality through controlled inhibitor release and self-healing characteristics. These gels are effective in maintaining protection over extended exposure times or after mechanical damage. Similarly, hydrogel and bio-based systems can contribute through crack sealing, ion adsorption, and in some cases biological mineralization. The reported performance varies widely, which might be due to differences in experimental conditions as well as evaluation techniques. So, the data in Table 2 should be defined as an overview of reported capabilities rather than a direct ranking. Therefore, the table shows the progression of gel coatings from simple barriers to complex gels that combine structural, chemical, and responsive mechanisms. The studies reviewed throughout this work reveal several common structure–property–performance relationships that govern the corrosion protection of gel-based coatings, regardless of the specific material system. Dense and highly crosslinked gels reduce pore connectivity and permeability, which can play a promising role in improving barrier performance. Strong adhesion suppresses defect formation. In addition, hydrophobic surface chemistry decreases water uptake. Encapsulated corrosion inhibitors and self-healing agents provide active protection by responding to coating damage. These design principles consistently emerge across conventional sol–gel coatings, polymer-gel composites, nanostructured systems, MOF-based coatings, and bio-inspired gels. So, superior corrosion performance can be achieved through the syn-

ergistic integration of passive barrier protection, active corrosion inhibition, and durable coating architecture.

Table 2. An overview of gels as corrosion protection coatings across different compositions. It should be noted that the electrochemical parameters were obtained under different research groups.

Gel/Coating System	Main Composition	Substrate/Medium	Key Results	Main Protection Mechanism	Ref.
TiO_2-SiO_2 multilayer sol–gel	TEOS/Ti alkoxide oxide network	Metallic substrate	Rp increased to 61 kΩ·cm^2 for three layers	Dense oxide barrier	[41]
Sol–gel + fluoride pretreatment	TEOS/GPTMS + hydroxyfluoride layer	WE54 Mg alloy	Pretreatment layer 600–900 nm; i_{corr} reduced to 1.37×10^{-8} A/cm^2	Interfacial stabilization + barrier	[45]
pH-controlled sol–gel	Silane-zirconium sol–gel	AA2024-T3/ 3.5% NaCl	pH 4: 71.8% Si-O-Si, Rct 8.42×10^5 Ω·cm^2, damaged area 3.2% after 960 h; pH 10: 40.23% Si-O-Si, 30.54% Si-OH, damaged area 54.9%	Network condensation control	[38]
TETA-crosslinked hybrid gel	GPTMS/TEOS/TETA	Metallic substrate	Gelation shortened from >90 days to <1–2 h; impedance 10^5–10^6 Ω·cm^2	Accelerated condensation + organic–inorganic crosslinking	[42]
Hybrid silica coating	MMA/MAPTMS/TEOS	AA2024-T3/0.1 M NaCl	Thickness 4 μm; impedance close to 1 GΩ·cm^2 after 6 months; no visible salt-spray damage after 500 h	Dense hybrid barrier	[53]
Zr-modified silica gel	TEOS/MAPTMS/ Zr + Ce^{3+}	Hot-dip galvanized steel/0.1 M NaCl	Initial impedance 10^7 Ω·cm^2, later 5×10^6 Ω·cm^2; optimum Ce^{3+} 650 ppm	Barrier + active Ce inhibition	[55]
Hydrophobic TEOS–polybenzoxazine gel	TEOS–PBz	Al alloy/3.5% NaCl	Thickness 0.5 μm; contact angle 105.6 ± 0.4°; Rct > 10^5 Ω·cm^2 after 1 week; benzoxazine conversion 94%	Hydrophobic dense barrier	[36]
ORMOSIL siloxane-polyacrylic coating	MAPTMS/acrylate/TEOS	Al alloy AA7075-T6 & 5% NaCl	Contact angle 70–85° for short chains, 90° for perfluoroalkyl coatings; impedance around 10 GΩ·cm^2 after 18 months; salt spray up to 550 h	Hybrid siloxane-polymer barrier	[57]
PATP-GPTMS ORMOSIL	GPTMS + p-aminothiophenol	Cu/3.5% NaCl	PATP concentration 0.001–0.1 M; efficiency 95.5% by EIS, 96.39% by polarization after 12 h	Si-O-Si barrier + Cu-S bonding	[61]
Bz/EP-modified sol–gel	Benzoxazine/epoxy/ sol–gel	Immersion test	Impedance > 10^6 Ω·cm^2 after 30 days; highly crosslinked systems > 10^8 Ω·cm^2; water absorption 1.29% after 1 day, up to 7.91% after 28 days at excessive curing	Multi-crosslinked hybrid barrier	[66]
WBPU/catecholamine/ sol–gel	WBPU + CAm/MPD sol–gel interlayer	Mg alloy/3.5% NaCl	Dry adhesion 1.74 to 2.75 MPa; wet adhesion 1.15 to 3.70 MPa; R_{ct} 4.9×10^4 to 1.7×10^7 Ω·cm^2 after 120 days; roughness 9.901 to 1.120 nm	Adhesion enhancement + pore sealing	[69]
Zr-MOG nanogel coating	Epoxy + Zr-MOG nanoparticles	3.5% NaCl	Surface area 455.7 m^2/g; pore diameter 1.2 nm; particle size 89 nm; healing efficiency 472.7%, 287.8%, 208.8% in acidic, neutral, alkaline media; impedance 259.69 to 135.69 kΩ·cm^2	pH-sensitive inhibitor release + barrier	[86]

Table 2. *Cont.*

Gel/Coating System	Main Composition	Substrate/Medium	Key Results	Main Protection Mechanism	Ref.
h-BN sol–gel sealing	PEO + functionalized h-BN	AA2024/0.1 M NaCl	h-BN 1000–2000 ppm; $R_{mix,in}$ 5.33×10^7 $\Omega \cdot cm^2$ after 1 week; capacitance 34.67 $nF \cdot cm^{-2}$ for poor dispersion; Si–O–Si/Si–OH ratio 1.86 to 2.42	Labyrinth barrier + network densification	[87]
O-MWCNT sol–gel	Silane gel + oxidized MWCNTs	NaCl	CNT loading 0.05%–0.9%; Si-O-Si/O-H ratio 2.22 to 9.02; thickness 1.59 ± 0.21 to 6.24 ± 0.35 µm; Rct 66.7 to 359.5 $k\Omega \cdot cm^2$; i_{corr} 5.40 to 0.04 $\mu A \cdot cm^{-2}$; ANN R^2 0.9879	Tortuous diffusion + Si-O-C bonding	[91]
Graphene nanosheet sol–gel	GPTMS/TEOS/silica/GN	AA2024-T3	Thickness 2.1–2.3 to 5.3–5.5 µm; roughness 0.5 to 3.6 nm; contact angle 74°; j_{corr} 3.0 ± 0.5 to 0.002 ± 0.001 $\mu A \cdot cm^{-2}$; E_{corr} −0.48 ± 0.03 to −0.32 V	Silica pore filling + graphene barrier	[92]
GO-filled sol–gel	PEO + sol–gel + GO	Ti6Al4V	Warburg resistance 1.60×10^6 $\Omega \cdot cm^2$; i_{corr} 1.17×10^{-7} to 1.88×10^{-8} $A \cdot cm^{-2}$; Ecorr 0.47 V; excessive GO: i_{corr} 2.85×10^{-8} $A \cdot cm^{-2}$, Ecorr 0.29 V	GO impermeable barrier	[93]
Nanodiamond sol–gel	Sol–gel + hydroxylated nanodiamond	Mg alloy	Optimum HND 0.01%; Rp 12.09 to 111.01 $k\Omega \cdot cm^2$; j_{corr} 2.202 to 0.476 $\mu A \cdot cm^{-2}$; Ecorr −1.519 to −1.335 V; 0.05% HND: j_{corr} 1.884 $\mu A \cdot cm^{-2}$	Compact barrier; excess filler causes defects	[94]
BTA@ZIF-8 sol–gel	ZIF-8 + BTA/2MI + sol–gel	AA2024-T3/3.5% NaCl	Thickness 2.6 µm; impedance 10^6 $\Omega \cdot cm^2$ after 30 days; degradation delayed from 3–14 days to 30 days; phase angle −50° vs. −10°; inhibitor loading 8.1%; adhesion > 20 MPa	MOF barrier + pH-triggered release	[82]
Cu-BTC MOF/ silica gel	Silica + Cu-BTC + 2-ABT	Ni–Fe alloy/3.5% NaCl	Loading 10.7 mg/100 mg MOF; release 40% in 24 h; j_{corr} 19.62 to 2.10 $\mu A \cdot cm^{-2}$; Ecorr −544.5 to −269.6 mV; Rp 1.57 to 11.69 to 74.6 $k\Omega \cdot cm^2$; porosity 0.3%; efficiency 98.87%	MOF nanocontainer + active adsorption	[101]
ZnO/ZIF-8@MBT sol–gel	MOF nanocontainer + MBT/2-MI	Damaged coating	ΔE −714 to 214 mV after 6 h; SF 1.15; adsorption energy −2.092 eV vs. −1.359 and −0.872 eV	Local self-healing + inhibitor co-adsorption	[105]
TGPG hydrogel microsphere/PAE	Tea polyphenol/GO/PVA microspheres + PAE	Salt spray/immersion	9.3×10^8 to 5×10^9 $\Omega \cdot cm^2$; stable after 28 days and 1000 h salt spray; swelling 1.2–1.3×; local temperature 46 °C; healed impedance 1×10^9 to 8×10^9 $\Omega \cdot cm^2$	multiple synergistic effects	[110]
PEO + inhibitor sol–gel sealing	BTA/8-HQ in PEO pores + sol–gel	0.1 M NaCl	Inhibitors 1–20 g/L; optimum 8-HQ/BTA 7:3; efficiency 93% after 72 h; thickness 12.8–13.4 µm; pores 1–10 µm; impedance > 10^8 $\Omega \cdot cm^2$ after 2 weeks	Inhibitor release + pore sealing	[115]
Supramolecular gel	Ethyl cellulose + imidazoline inhibitors	3.5% NaCl	Inhibitor loading up to 25%; C17 efficiency 91% at 10×10^{-4} mol/L; Ecorr shift −621 to −451 mV and −557 to −493 mV after 7 days	Hydrophobic adsorption film + self-healing	[26]
Magnetic supramolecular gel	Supramolecular gel + 10% Fe_3O_4	Damaged coating	Heating near 80 °C; rate 1.64 °C/s; defect closure within 58 s; repeated healing up to 10 cycles	Externally triggered healing	[116]

Table 2. *Cont.*

Gel/Coating System	Main Composition	Substrate/Medium	Key Results	Main Protection Mechanism	Ref.
pH-responsive BTA-ZIF-8/BN gel	BTA-ZIF-8 + BN-OH + sol–gel	Al alloy	Low-frequency impedance 2×10^8 Ω·cm^2 after 28 days; about 3 orders higher than unmodified sol–gel	Labyrinth barrier + pH-triggered release	[25]
g-C_3N_4@LP sol–gel	Losartan-loaded g-C_3N_4 nanoplates	Immersion	Size 803 nm; additive 100 ppm; roughness 1.77 to 1.60 µm; Rp 1.782 MΩ·cm^2 after 120 h, >18× unmodified coating; release stabilizes after 1 h at pH 10–12	pH-responsive inhibitor release	[120]
TBP gel/epoxy	TA/BTA/polymer gel in epoxy	Long-term immersion	Impedance 2.36×10^7 Ω·cm^2 after 181 days; neat epoxy 6.86×10^4 Ω·cm^2; dry adhesion +18.2%, wet adhesion +74.7%	Swelling repair + inhibitor release	[121]
PVA gel sensing electrolyte	PVA gel electrolyte	Cu/Ag corrosion sensing	Ionic conductivity 11.44 mS·cm^{-1} at 0.1 M KCl and 2.00 mS·cm^{-1} at 0.01 M KCl; potential near −10 mV; Cu_2O thickness 2.13 vs. 2.19 µm; Ag_2S 723/694 vs. 689 nm; stable up to 48 h	Flexible corrosion monitoring	[122]
PDMS/SiO_2 gel coating	PDMS + 0%–20% SiO_2	Steel rebar/concrete pore solution	Optimum 15% SiO_2; inhibition efficiency 95.8%; crack-free after 24 h	Dense polymer–silica barrier	[132]
PVB/silica gel coating	PVB + silica	Rebar/simulated pore solution	Young's modulus 36.3 to 94.5 MPa with 15% silica; optimum 10% silica; efficiency 89.3% after 2 days	Mechanical strengthening + barrier	[133]
MICP bio-gel crack repair	Bacteria + calcium alginate	Reinforced concrete	Adsorption 118.3 mg/g, 31.6% higher than alginate; crack sealing up to 1 mm in 15 min; i_{corr} 2.88×10^{-6} mA·cm^{-2}; corrosion reduction 88.7%	Crack sealing + chloride binding + $CaCO_3$ densification	[29]
Calcium alginate gel repair	Calcium alginate	Cracked concrete	Rp 3109 to 1799 Ω·cm^2 after 14 days; i_{corr} 0.073 to 0.0928 µA·cm^{-2}	Physical sealing	[29]
Bio-gel CAB repair	Calcium alginate + bacteria	Cracked concrete	Rp 4890 to 3847 Ω·cm^2 after 14 days; i_{corr} 0.1151 to 0.1988 µA·cm^{-2}	Bio-mineral sealing + chloride binding	[29]
Untreated cracked concrete	No gel	Cracked concrete	Rp 555 to 433 Ω·cm^2; i_{corr} 0.6425 to 0.8244 µA·cm^{-2} after 14 days	Baseline deterioration	[29]
Alkaline hydrogel crack repair	Diallyldimethylammonium hydroxide/acrylic acid hydrogel	Concrete cracks	No water penetration for >28 days	Crack sealing + alkalinity restoration + steel re-passivation	[134]
Bacillus/biosurfactant bio-gel	Silica sol–gel + Bacillus clausii/biosurfactant	Steel/MIC environment	Spore survival 20.8%, 1.71×10^6 CFU/mL; contact angle 60.6° to 93.25°/83.22°; bacterial population 2.23×10^5 CFU/mL; biofilm delay 12 days; i_{corr} 0.51 µA/cm^2 after 180 days; impedance 10^4 Ω·cm^2	Antimicrobial barrier + biofilm suppression	[139]
Clitoria ternatea bio-gel	Plant extract + silica sol–gel	Steel	Extract 75 ppm; i_{corr} 618 to 64.2 µA·cm^{-2}; efficiency 89.6% ethanol extract and 85.6% water extract; Rct 488 Ω·cm^2; Fe retention 92% vs. 68.67%	Bioactive adsorption + Fe–O–Si bonding	[140]
Caffeine sol–gel	TEOS/APTES + caffeine	Steel	Caffeine 25–100 ppm; Rct 2441.65 to 6218.02 Ω·cm^2; efficiency 84.22–88.79%; i_{corr} 6.3096 to 0.7079 µA·cm^{-2}; noise resistance 0.23 to 1.83 kΩ·cm^2; Fe 85.44%, Cl 0.12%; contact angle 59.74° to 96.41°	Green inhibitor adsorption + hydrophobic barrier	[142]

Table 2. *Cont.*

Gel/Coating System	Main Composition	Substrate/Medium	Key Results	Main Protection Mechanism	Ref.
Lignin-based hybrid gel	Organosilane/Zr + 3% lignin/NADES	Al2024	Lignin 3%; room temperature curing; thinner coating but improved corrosion resistance	Sustainable crosslinking + barrier	[147]

Table 2 demonstrates that the impedance values range from 10^4 to over 10^9 $\Omega \cdot cm^2$ depending on coating composition and protection mechanism. These variations cannot be attributed to a single material component but to the combined effects of network crosslinking density, coating compactness, adhesion, hydrophobicity, incorporation of functional nanofillers, and active corrosion inhibition. Conventional gel coatings generally exhibit impedance values in the range of $10^{5-}10^7$ $\Omega \cdot cm^2$ because their protection primarily depends on passive barrier properties. In contrast, highly crosslinked hybrid organic–inorganic coatings, ORMOSIL systems, and multilayer architectures often achieve impedance values approaching or exceeding $10^{8-}10^9$ $\Omega \cdot cm^2$ owing to their dense siloxane networks, reduced porosity, and superior resistance to water and chloride ion penetration. Other improvements are observed in multifunctional gel coatings incorporating nanomaterials or other inhibitors. Graphene oxide, hexagonal boron nitride, carbon nanotubes, nanodiamonds, and silica nanoparticles increase the tortuosity of diffusion pathways, effectively delaying electrolyte transport through the coating. MOFs provide an additional active protection mechanism by functioning as nanocontainers for the controlled release of corrosion inhibitors in response to local environmental changes such as pH variation. The highest impedance values reported in Table 2 are generally associated with multifunctional coating systems that combine dense barrier structures with active inhibitor release, self-healing, and strong adhesion, whereas lower impedance values are observed for coatings relying solely on passive barrier protection or structural defects that facilitate electrolyte ingress.

9. Conclusions and Future Challenges

This review introduced gel coating studies to mitigate corrosion and increase the durability of metal substrates. The literature review indicates that gel coatings can reduce corrosion current density and increase charge transfer resistance compared to uncoated substrates. Such improvements can be attributed to the formation of dense, crosslinked hybrid networks that retard ionic transport and moisture penetration. In addition, the incorporation of inhibitors and nanofillers in gel coatings has been reported to decrease chloride diffusion coefficients. Self-healing gels enhanced performance via improving barrier properties. In short, the reviewed gel coatings are better than conventional coatings in terms of durability, adhesion strength, and electrochemical stability. However, performance variability under real conditions suggests that further optimization is required before large-scale uses.

Despite promising laboratory-scale results, several challenges are discussed regarding the use of these coatings in industry. The first critical issue is long-term durability under coupled environmental stressors. Another key challenge is scalability and cost. Many gels can be prepared using expensive alkoxide precursors and controlled synthesis conditions. Developing low-cost precursors and simplified processing methods will be essential for gel commercialization. The efficiency of self-healing systems also requires further improvement. Although initial healing efficiencies can exceed 80%, repeated damage cycles often lead to a reduction below 50%. Future work should focus on multi-cycle healing capability and controlled release mechanisms. Standardization remains a big gap in the research on corrosion. Variations in evaluation methods make direct comparison between studies diffi-

cult. Finally, the sustainability factor should be considered in future research. Developing smart sensing technologies for real-time corrosion monitoring could enhance the functionality of the gel coatings. Addressing these challenges through interdisciplinary research will be crucial for transport gel-based coating technologies from laboratory innovation to industry.

The future of gels in corrosion science is predicted to go in the direction of intelligent multifunctional systems. These systems combine self-healing, ion sensing, and monitor changes in gel structures. Advances in materials and natural extracts will improve durability and sustainability. Furthermore, the integration of artificial intelligence and machine learning offers a promising opportunity to achieve fast design and optimization steps. Emerging manufacturing technologies such as additive manufacturing and digital fabrication may also enable the production of gels with controlled characteristics. Future research can additionally emphasize long-term large-scale validation, life-cycle assessment, and the development of electrochemical testing to facilitate fast comparison among different gels. In conclusion, these advances will accelerate the transition of gel coatings from laboratory-scale to commercially sustainable and intelligent corrosion protection technologies.

Author Contributions: Conceptualization, I.M.A.M. and H.M.A.E.-L.; software, I.M.A.M.; writing—original draft preparation, I.M.A.M. and H.M.A.E.-L.; writing—review and editing, I.M.A.M. and H.M.A.E.-L.; visualization, I.M.A.M. and H.M.A.E.-L.; supervision, I.M.A.M. and H.M.A.E.-L.; project administration, H.M.A.E.-L.; funding acquisition, H.M.A.E.-L. All authors have read and agreed to the published version of the manuscript.

Funding: This work was supported by the Deanship of Scientific Research, Vice Presidency for Graduate Studies and Scientific Research at King Faisal University, Saudi Arabia (Grant No. KFU264008).

Data Availability Statement: Data is contained within the article.

Conflicts of Interest: The authors declare no conflicts of interest.

Abbreviations

The following abbreviations are used in this manuscript:

GPTMS	3-glycidoxypropyltrimethoxysilane
TEOS	Tetraethylorthosilicate
ORMOSIL	Organic-modified silicate
TETA	Triethylenetetramine
MAPTMS	3-methacryloxypropyl trimethoxysilane
BZ/EP	Benzoxazine/epoxy
WBPU	Waterborne polyurethane
MICP	Induced calcium carbonate precipitation
MOG	Metal–organic gel
CAm	Catecholamine
h-BN	Hexagonal boron nitride
2-ABT	2-aminobenzothiazol
BTA	Benzotriazole
PEO	Plasma electrolytic oxidation
PVB	Polyvinyl butyral
DLS	Dynamic light-scattering
J_{corr}	Corrosion current density
NADES	natural deep eutectic solvent
FTIR	Fourier transform infrared spectroscopy
XPS	X-ray photoelectron spectroscopy
SEM	Scanning electron microscopy
AFM	Atomic force microscopy

CA	Contact angle
PD	Potentiodynamic polarization
GD-OES	Glow discharge optical emission spectroscopy
EIS	Electrochemical impedance spectroscopy
NaCl	Sodium chloride
PVA	Poly(vinyl alcohol)
RC	Reinforced concrete
Rct	Charge transfer resistance
Rs	Solution resistance
i_{corr}	Corrosion current density
Rp	Polarization resistance
HDGS	Hot-dip galvanized steel
Rt	Residence time
RL	Layer resistance

References

1. Zhu, Y.J.; Bi, C.X.; Zhao, M.; Li, Z.; Feng, W.J.; Sun, F.; Zhang, X.Q.; Li, B.Q.; Huang, J.Q. Deciphering the Species-Dependent Polysulfide Corrosion on Lithium Anode Toward Durable Lithium–Sulfur Batteries. *Adv. Mater.* **2025**, *37*, e2506132. [CrossRef] [PubMed]
2. Fincher, C.D.; Gilgenbach, C.; Roach, C.; Osmundsen, R.; Penn, A.; Thouless, M.D.; Carter, W.C.; Sheldon, B.W.; LeBeau, J.M.; Chiang, Y.-M. Electrochemical corrosion accompanies dendrite growth in solid electrolytes. *Nature* **2026**, *652*, 906–911. [CrossRef] [PubMed]
3. Yu, Z.; Sun, Y.; Wu, H.; Guo, F.; Hu, J.; Liu, M.; Zhou, X.; Wu, H.; Hu, J.; Wang, L.; et al. Anodic protection enables moisture-stable Mg3(Sb, Bi)2 for thermoelectric cooling. *Nat. Mater.* **2026**, *25*, 1182–1189. [CrossRef] [PubMed]
4. Rana, Z.; Olivares, D.; Marzo, A.; Jiménez-Arévalo, V.M.; Fuentealba, E.; Rabanal-Arabach, J.; Galleguillos Madrid, F.M. Accelerated corrosion performance of solar cells: A critical review. *Sol. Energy Mater. Sol. Cells* **2026**, *297*, 114103. [CrossRef]
5. Rao, S.G.; Yao, Y.; Törne, K.; Mølmen, L.; Nederstedt, H.; Leisner, P.; Lundblad, A.; Kubart, T. Corrosion resistance of coated aluminum bipolar plates for proton exchange membrane fuel cells. *Electrochim. Acta* **2025**, *539*, 146966. [CrossRef]
6. Wang, Q.; Wang, Z.; Li, C.; Qiao, X.; Guan, H.; Zhou, Z.; Song, D. Research progress in corrosion behavior and anti-corrosion methods of steel rebar in concrete. *Metals* **2024**, *14*, 862. [CrossRef]
7. Charpentier Poncelet, A.; Helbig, C.; Loubet, P.; Beylot, A.; Muller, S.; Villeneuve, J.; Laratte, B.; Thorenz, A.; Tuma, A.; Sonnemann, G. Losses and lifetimes of metals in the economy. *Nat. Sustain.* **2022**, *5*, 717–726. [CrossRef]
8. Hao, S.; Hou, S.; Nan, D.; Xu, D.; Shen, W.; Kang, F.; Huang, Z.-H. PH-Sensitive Self-Healing Waterborne Epoxy Coating: Polydopamine Grafted Graphene Oxide with 2-Mercaptobenzimidazole Inhibitors and Cerium Cation Towards Anti-Corrosion Performance. *Polymers* **2026**, *18*, 459. [CrossRef] [PubMed]
9. Yu, C.; Wei, M.; Wang, Q.; Zhang, W. Spatial Tribological Properties of PI/PTFE Based Self-Stratifying Composite Coatings Grafted by Amino-POSS. *Polymers* **2026**, *18*, 521. [CrossRef] [PubMed]
10. Nakata, T.; Xu, C.; binti Osman, N.A.S.; Geng, L.; Kamado, S. Development of corrosion-resistant Mg-Al-Ca-Mn-Zn alloy sheet with good tensile properties and stretch formability. *J. Alloys Compd.* **2022**, *910*, 164752. [CrossRef]
11. Abd El-Lateef, H.M.; Basubaih, M.A.O.; Gouda, M.; Shalabi, K.; Mohamed, I.M. Eco-friendly carbohydrate nanocomposites of amino cellulose and MWCNTs for high-performance corrosion protection of construction steel alloys. *Constr. Build. Mater.* **2025**, *475*, 141219. [CrossRef]
12. Wang, K.; Song, B.; Wei, J.; Cao, W.; Zhang, L.; Zheng, H.; Li, W.; Redaelli, E.; Li, W. A review of the development of photoelectrochemical cathodic protection from the perspective of hole scavengers and interface synergy. *Chem. Eng. J.* **2025**, *521*, 167000. [CrossRef]
13. Zhu, J.-H.; Wu, X.-Y.; Mohamed, I.M.A.; Xing, F. Electrochemical and microstructural evaluation of acidification damage induced by impressed current cathodic protection after incorporating a hydroxy activated-Mg/Al-double oxide in the external anode mortar. *Constr. Build. Mater.* **2021**, *309*, 125116. [CrossRef]
14. Motlatle, A.M.; Ray, S.S.; Ojijo, V.; Scriba, M.R. Polyester-Based Coatings for Corrosion Protection. *Polymers* **2022**, *14*, 3413. [CrossRef] [PubMed]
15. Kessler, V.G.; Seisenbaeva, G.A. Molecular mechanisms of the metal oxide sol-gel process and their application in approaches to thermodynamically challenging complex oxide materials. *J. Sol-Gel Sci. Technol.* **2023**, *107*, 190–200. [CrossRef]
16. Ciriminna, R.; Fidalgo, A.; Pandarus, V.; Béland, F.; Ilharco, L.M.; Pagliaro, M. The Sol–Gel Route to Advanced Silica-Based Materials and Recent Applications. *Chem. Rev.* **2013**, *113*, 6592–6620. [CrossRef] [PubMed]

17. Chelu, M.; Musuc, A.M. Polymer gels: Classification and recent developments in biomedical applications. *Gels* **2023**, *9*, 161. [CrossRef] [PubMed]
18. Su, Y.; Wang, Z.; Legrand, A.; Aoyama, T.; Ma, N.; Wang, W.; Otake, K.-I.; Urayama, K.; Horike, S.; Kitagawa, S.J. Hypercrosslinked polymer gels as a synthetic hybridization platform for designing versatile molecular separators. *J. Am. Chem. Soc.* **2022**, *144*, 6861–6870. [CrossRef] [PubMed]
19. Liu, Y.; Zhao, C.; Xiong, Y.; Yang, J.; Jiao, H.; Zhang, Q.; Cao, R.; Wang, Z.L.; Sun, Q. Versatile ion-gel fibrous membrane for energy-harvesting iontronic skin. *Adv. Funct. Mater.* **2023**, *33*, 2303723. [CrossRef]
20. Wang, Z.; Qiu, W.; Zhang, Q. Constructing phase separation in polymer gels: Strategies, functions and applications. *Prog. Polym. Sci.* **2024**, *154*, 101847. [CrossRef]
21. Huang, W.-H.; Lin, C.-S. Robust superhydrophobic transparent coatings fabricated by a low-temperature sol–gel process. *Appl. Surf. Sci.* **2014**, *305*, 702–709. [CrossRef]
22. Basso, M.; Colusso, E.; Carraro, C.; Kalha, C.; Riaz, A.A.; Bombardelli, G.; Napolitani, E.; Chen, Y.; Jasieniak, J.; Ratcliff, L.E.; et al. Rapid laser-induced low temperature crystallization of thermochromic VO2 sol-gel thin films. *Appl. Surf. Sci.* **2023**, *631*, 157507. [CrossRef]
23. Minakov, A.V.; Pryazhnikov, M.I.; Neverov, A.L.; Sukhodaev, P.O.; Lysakova, E.I.; Skorobogatova, A.D. A systematic study of the effect of nano-additives on the functional characteristics of hydraulic fracturing gels. *Colloids Surf. A Physicochem. Eng. Asp.* **2024**, *702*, 135057. [CrossRef]
24. Kim, D.; Liu, X.; Yu, B.; Mateti, S.; O'Dell, L.A.; Rong, Q.; Chen, Y. Amine-Functionalized Boron Nitride Nanosheets: A New Functional Additive for Robust, Flexible Ion Gel Electrolyte with High Lithium-Ion Transference Number. *Adv. Funct. Mater.* **2020**, *30*, 1910813. [CrossRef]
25. Huang, Y.; Zhao, C.; Li, Y.; Wang, C.; Yuan, W.; Shen, T.; Liu, J.; Cheng, D.; Wu, C.; Shen, Q.; et al. A smart sol-gel coating incorporating pH-responsive BTA-ZIF-8 MOF assembled hexagonal boron nitride for active/passive corrosion protection of 1060 aluminum alloy. *Surf. Coat. Technol.* **2023**, *474*, 130072. [CrossRef]
26. Lin, B.; Wang, J.; Zhang, H.; Wang, Y.; Zhang, H.; Tang, J.; Hou, J.; Zhang, H.; Sun, M. Self-healing performance of ethyl-cellulose based supramolecular gel coating highly loaded with different carbon chain length imidazoline inhibitors in NaCl corrosion medium. *Corros. Sci.* **2022**, *197*, 110084. [CrossRef]
27. Huang, Y.; Zhao, C.; Li, Y.; Wang, C.; Shen, T.; Cheng, D.; Yang, H. Development of self-healing sol-gel anticorrosion coating with pH-responsive 1H-benzotriazole-inbuilt zeolitic imidazolate framework decorated with silica shell. *Surf. Coat. Technol.* **2023**, *466*, 129622. [CrossRef]
28. Gu, K.; Lv, L.; Lu, Z.; Yang, H.; Mao, F.; Tang, J. Electrochemical corrosion and impedance study of SAE1045 steel under gel-like environment. *Corros. Sci.* **2013**, *74*, 408–413. [CrossRef]
29. Fan, Q.; Fan, L.; Quach, W.-M.; Duan, J. Investigation of a bio-gel for concrete crack repair and corrosion inhibition of steel bars. *Corros. Sci.* **2025**, *256*, 113228. [CrossRef]
30. Li, H.; Lyamina, G.; Gou, P.; Ke, W.; Dubinina, O. Chitosan/Glycerol Gel Films for the Accurate In Vitro Evaluation of the Corrosion of Biodegradable Medical Magnesium Alloys. *Mater. Proc.* **2026**, *29*, 4. [CrossRef]
31. Lopez-Martinez, E.; Arrabal, R.; Pillado, B.; Matykina, E.; Vega, J.M.; Mohedano, M. Multilayer PEO/Sol-gel systems doped with inorganic inhibitors for the corrosion protection of AZ31B alloy. *Prog. Org. Coat.* **2026**, *214*, 109996. [CrossRef]
32. Merino, E.; Durán, A.; Ceré, S.; Castro, Y. Hybrid Epoxy-Alkyl Sol–Gel Coatings Reinforced with SiO2 Nanoparticles for Corrosion Protection of Anodized AZ31B Mg Alloy. *Gels* **2022**, *8*, 242. [CrossRef] [PubMed]
33. Fan, S.; Sun, X.; Peng, M.; Duan, Y.; Li, J.; Zheng, S.; Li, M. Fabrication of highly corrosion-resistant Zn-Cu-Ti alloy coatings via anodization and gel-assisted electrophoretic deposition and study of their corrosion properties. *Surf. Interfaces* **2026**, *83*, 108544. [CrossRef]
34. Jafari-Tarzanagh, Y.; Seifzadeh, D.; Khodayari, A.; Samadianfard, R. Active corrosion protection of AA2024 aluminum alloy by sol-gel coating containing inhibitor-loaded mesoporous SBA-15. *Prog. Org. Coat.* **2022**, *173*, 107166. [CrossRef]
35. Fan, Y.; Mu, S.; Ou, Y.; Guo, J.; Du, J.; Zhang, G. Influence of different inhibitors on the conductive and corrosion resistance performance of sol–gel coatings on 6063 aluminum alloy. *Appl. Surf. Sci.* **2025**, *708*, 163696. [CrossRef]
36. Zhou, Z.; Li, C.; Wang, R.; Tao, H.; Yang, D.; Qin, S.; Meng, X.; Zhou, C. Crosslinking control of hydrophobic benzoxazine-based hybrid sol-gel coating for corrosion protection on aluminum alloys. *Prog. Org. Coat.* **2022**, *171*, 107059. [CrossRef]
37. Hu, H.; Huang, X.; Chen, J.; Chen, J. PVA/PEGDA microgels loaded with L-cysteine for corrosion inhibition coating on fragile bronze. *J. Coat. Technol. Res.* **2025**, *22*, 631–649. [CrossRef]
38. Chen, C.; Yu, M.; Zhan, Z.; Ge, Y.; Sun, Z.; Liu, J. Effect of pH on the structure and corrosion protection properties of sol-gel coatings. *Corros. Sci.* **2023**, *212*, 110955. [CrossRef]
39. Yang, Y.; Zhu, Y.; Yan, Z.; Cao, D.; Song, Y.; Zheng, Y.; Wu, Y.; Yue, J.; Cao, J.; Li, S. Strategic microstructure manipulation of porous materials for advanced corrosion protection in metallic alloys. *Chem. Sci.* **2025**, *16*, 22250–22265. [CrossRef] [PubMed]

40. Schubert, U. En route from metal alkoxides to metal oxides: Metal oxo/alkoxo clusters. *J. Sol-Gel Sci. Technol.* **2023**, *105*, 587–595. [CrossRef]
41. Khosravi, H.S.; Veerapandiyan, V.K.; Vallant, R.; Reichmann, K. Effect of processing conditions on the structural properties and corrosion behavior of TiO2–SiO2 multilayer coatings derived via the sol-gel method. *Ceram. Int.* **2020**, *46*, 17741–17751. [CrossRef]
42. Perrin, F.X.; Ziarelli, F.; Dupuis, A. Relation between the corrosion resistance and the chemical structure of hybrid sol-gel coatings with interlinked inorganic-organic network. *Prog. Org. Coat.* **2020**, *141*, 105532. [CrossRef]
43. Wang, Z.; Li, L.; Jia, F.; Wu, J.; Jin, W.; Zhao, W.; Cao, J.; Cheng, Y.; Shi, L.; Yun, S.; et al. Exploring the effect of pH-shifting on the gel properties and interaction of heat-induced Flammulina velutipes polysaccharide-porcine myofibrillar protein for improving the quality of Flammulina velutipes-pork patties. *Food Chem.* **2025**, *465*, 142187. [CrossRef] [PubMed]
44. Khalesi, F.; Farhadian, M.; Raeissi, K. Porosity tailoring of electrophoretically derived zirconia coatings using acidic and alkaline-based sol-gel post-treatment to enhance anti-corrosion performance. *Surf. Coat. Technol.* **2021**, *425*, 127692. [CrossRef]
45. Durán, K.S.; Hernández-Barrios, C.A.; Coy, A.E.; Viejo, F. Effect of fluoride conversion pretreatment time and the microstructure on the corrosion performance of TEOS-GPTMS sol–gel coatings deposited on the WE54 magnesium alloy. *J. Mater. Res. Technol.* **2021**, *15*, 4220–4242. [CrossRef]
46. Mahadevan, T.S.; Kalahe, J.; Du, J. Temperature effect on structural evolution of aluminosilicate gels formed during borosilicate nuclear waste glass corrosion. *J. Non-Cryst. Solids* **2025**, *663*, 123573. [CrossRef]
47. Figueira, R.B.; Silva, C.J.R.; Pereira, E.V. Influence of Experimental Parameters Using the Dip-Coating Method on the Barrier Performance of Hybrid Sol-Gel Coatings in Strong Alkaline Environments. *Coatings* **2015**, *5*, 124–141. [CrossRef]
48. Aslan Çakır, M.; Yetim, T.; Yetim, A.F.; Çelik, A. Superamphiphobic TiO2 Film by Sol–Gel Dip Coating Method on Commercial Pure Titanium. *J. Mater. Eng. Perform.* **2024**, *33*, 1472–1484. [CrossRef]
49. Valet, S.; Burkert, A.; Ebell, G.; Babutzka, M. Determination of the corrosion product layer resistance on zinc and electrolytically galvanized steel samples by using gel electrolytes. *Electrochim. Acta* **2021**, *385*, 138191. [CrossRef]
50. Hou, Y.; Zhu, G.; Cui, J.; Wu, N.; Zhao, B.; Xu, J.; Zhao, N. Superior Hard but Quickly Reversible Si–O–Si Network Enables Scalable Fabrication of Transparent, Self-Healing, Robust, and Programmable Multifunctional Nanocomposite Coatings. *J. Am. Chem. Soc.* **2022**, *144*, 436–445. [CrossRef] [PubMed]
51. Xu, Q.; Zhang, S.; Wang, K.; Chen, L.; Nie, J.; Xu, Z.; Jiang, M.; Liu, P. Novel Multifunction Epoxy Thermoset Designed by Manipulating the Silicon-Oxidation Flexible-Rigid Network Topology: Toughening, Strengthening, and Acid/Alkali Resistance. *Ind. Eng. Chem. Res.* **2023**, *62*, 14743–14754. [CrossRef]
52. Wang, Y.; Liang, M.; Tong, B.; Wang, Y.; Han, Z.; Zhang, X. Interfacial Si-O-Si network construction for high-performance Si3N4@SiO2/polyurethane composites in thermal management. *Ceram. Int.* **2026**, *52*, 11170–11180. [CrossRef]
53. Rodič, P.; Lekka, M.; Andreatta, F.; Fedrizzi, L.; Milošev, I. The effect of copolymerisation on the performance of acrylate-based hybrid sol-gel coating for corrosion protection of AA2024-T3. *Prog. Org. Coat.* **2020**, *147*, 105701. [CrossRef]
54. Suárez-Vega, A.; Agustín-Sáenz, C.; O'Dell, L.A.; Brusciotti, F.; Somers, A.; Forsyth, M. Properties of hybrid sol-gel coatings with the incorporation of lanthanum 4-hydroxy cinnamate as corrosion inhibitor on carbon steel with different surface finishes. *Appl. Surf. Sci.* **2021**, *561*, 149881. [CrossRef]
55. Nguyen, T.T.; Thai, T.T.; Paint, Y.; Trinh, A.T.; Olivier, M.-G. Effect of cerium nitrate concentration on corrosion protection of hybrid organic/inorganic Si/Zr sol-gel coating applied on hot-dip galvanized steel. *Surf. Coat. Technol.* **2024**, *480*, 130562. [CrossRef]
56. Hamulić, D.; Medoš, G.; Korte, D.; Rodič, P.; Milošev, I. The Effect of Curing Temperature and Thickness of Polybutyl Methacrylate Siloxane Coatings on the Corrosion Protection of Structural Steel S355. *Coatings* **2023**, *13*, 675. [CrossRef]
57. Milošev, I.; Hamulić, D.; Rodič, P.; Carrière, C.; Zanna, S.; Budasheva, H.; Korte, D.; Franko, M.; Mercier, D.; Seyeux, A.; et al. Siloxane polyacrylic sol-gel coatings with alkly and perfluoroalkyl chains: Synthesis, composition, thermal properties and log-term corrosion protection. *Appl. Surf. Sci.* **2022**, *574*, 151578. [CrossRef]
58. Liu, Z.; Tian, S.; Li, Q.; Wang, J.; Pu, J.; Wang, G.; Zhao, W.; Feng, F.; Qin, J.; Ren, L. Integrated Dual-Functional ORMOSIL Coatings with AgNPs@rGO Nanocomposite for Corrosion Resistance and Antifouling Applications. *ACS Sustain. Chem. Eng.* **2020**, *8*, 6786–6797. [CrossRef]
59. Jaswal, N.; Aman; Bahadur, V.; Kumar, P. ORMOSIL: Advanced catalytic application in organic synthesis. *J. Iran. Chem. Soc.* **2025**, *22*, 931–953. [CrossRef]
60. Zhang, X.; Ou, S.; Zhang, L.; Tan, J.; Lin, W.; Li, R.; Yuan, Z. Robust superhydrophobic ORMOSIL hybrid coating via chemical-assembly engineering for wood protection. *Adv. Compos. Hybrid Mater.* **2025**, *8*, 217. [CrossRef]
61. Balaji, J.; Roh, S.-H.; Edison, T.N.J.I.; Jung, H.-Y.; Sethuraman, M.G. Sol-gel based hybrid silane coatings for enhanced corrosion protection of copper in aqueous sodium chloride. *J. Mol. Liq.* **2020**, *302*, 112551. [CrossRef]
62. Saavedra-Torres, M.; Jaque, P.; Tielens, F.; Santos, J.C. Theoretical study of dibenzyl disulfide adsorption on Cu7 cluster as a first approximation to sulfur-induced copper corrosion process. *Theor. Chem. Acc.* **2015**, *134*, 73. [CrossRef]
63. Figueira, R.B. Hybrid Sol–gel Coatings for Corrosion Mitigation: A Critical Review. *Polymers* **2020**, *12*, 689. [CrossRef] [PubMed]

64. Bifulco, A.; Imparato, C.; Aronne, A.; Malucelli, G. Flame retarded polymer systems based on the sol-gel approach: Recent advances and future perspectives. *J. Sol-Gel Sci. Technol.* **2025**, *115*, 226–250. [CrossRef]
65. Li, J.; Li, T.; Zeng, Y.; Chen, C.; Guo, H.; Lei, B.; Zhang, P.; Feng, Z.; Meng, G. A novel sol-gel coating via catechol/lysine polymerization for long-lasting corrosion protection of Mg alloy AZ31. *Colloids Surf. A Physicochem. Eng. Asp.* **2023**, *656*, 130361. [CrossRef]
66. Song, S.; Zhang, H.; Wan, H.; Wang, W.; Xin, Z.; Liu, J.; Zhou, C. Dual-functional benzoxazine/epoxy composite modified sol-gel coating for corrosion protection and antibacterial applications. *Prog. Org. Coat.* **2026**, *212*, 109840. [CrossRef]
67. Mohan, S.; Subramani, D.; Ammasai, K.; Muthukaruppan, A. Imidazole-core polybenzoxazine-silica hybrid composites via sol-gel approach: A new strategy for superior corrosion and flame resistance. *Next Mater.* **2025**, *9*, 101348. [CrossRef]
68. Su, Q.; Sun, Y.; Li, J.; Ma, B.; Zhang, X.; Tian, H.; Ju, Y.; Gao, S.; Liu, Z.; Zhang, T.; et al. Supramolecular Engineering of a Homo[2]catenane Filler Enables Polymer Composites with Exceptional High-Temperature Capacitive Energy Storage. *Molecules* **2026**, *31*, 1691. [CrossRef] [PubMed]
69. Li, J.; Wang, L.; Bai, H.; Chen, C.; Liu, L.; Guo, H.; Lei, B.; Meng, G.; Yang, Z.; Feng, Z. Development of an eco-friendly waterborne polyurethane/catecholamine/sol-gel composite coating for achieving long-lasting corrosion protection on Mg alloy AZ31. *Prog. Org. Coat.* **2023**, *183*, 107732. [CrossRef]
70. Myasoedova, T.N.; Kalusulingam, R.; Mikhailova, T.S. Sol-Gel Materials for Electrochemical Applications: Recent Advances. *Coatings* **2022**, *12*, 1625. [CrossRef]
71. Huang, Y.; Zhao, C.; Li, Y.; Wang, C.; Shen, T.; Wu, C.; Hu, Z.; Cheng, D.; Yang, H. Enhanced corrosion resistance and self-healing effect of sol–gel coating incorporating one-pot-synthesized corrosion inhibitor-encapsulated silica nanocontainers. *J. Sol-Gel Sci. Technol.* **2022**, *104*, 78–90. [CrossRef]
72. Zhenzhen, W.; Chunming, O.; Zhihui, F.; Yongcun, M.; Shusen, P. Preparation of γ-GPS-ZrO2 hybrid coating by sol-gel method and its synergistic enhancement effect on corrosion resistance and adhesion of AA2024 aluminum alloy. *J. Sol-Gel Sci. Technol.* **2025**, *116*, 1432–1450. [CrossRef]
73. Wang, Z.; Xiao, J.; Zhao, T.; Zhang, C.; Wang, L.; He, N.; Kong, Q.; Wang, X. Transient regulation of gel properties by chemical reaction networks. *Chem. Commun.* **2023**, *59*, 9818–9831. [CrossRef] [PubMed]
74. Guaragnone, T.; Rossi, M.; Chelazzi, D.; Mastrangelo, R.; Severi, M.; Fratini, E.; Baglioni, P. pH-Responsive Semi-Interpenetrated Polymer Networks of pHEMA/PAA for the Capture of Copper Ions and Corrosion Removal. *ACS Appl. Mater. Interfaces* **2022**, *14*, 7471–7485. [CrossRef] [PubMed]
75. Wang, M.; Nie, C.; Liu, J.; Wu, S. Organic–inorganic semi-interpenetrating networks with orthogonal light- and magnetic-responsiveness for smart photonic gels. *Nat. Commun.* **2023**, *14*, 1000. [CrossRef] [PubMed]
76. Guohua, L.; Zhiyong, Z.; Yangang, W. Research progress on highly conductive polymer composites based on carbon-based nanofillers. *Polym. Compos.* **2025**, *46*, 9742–9775. [CrossRef]
77. Mao, T.; Li, C.; Mao, F.; Xue, Z.; Xu, G.; Amirfazli, A. A durable anti-corrosion superhydrophobic coating based on carbon nanotubes and SiO2 aerogel for superior protection for Q235 steel. *Diam. Relat. Mater.* **2022**, *129*, 109370. [CrossRef]
78. Sfameni, S.; Del Tedesco, A.; Rando, G.; Truant, F.; Visco, A.; Plutino, M.R. Waterborne Eco-Sustainable Sol–Gel Coatings Based on Phytic Acid Intercalated Graphene Oxide for Corrosion Protection of Metallic Surfaces. *Int. J. Mol. Sci.* **2022**, *23*, 12021. [CrossRef] [PubMed]
79. Mirche, K.K.; Pandey, K.K.; Pandey, S.M.; Keshri, A.K. Microstructure and Corrosion Behavior of Plasma-Sprayed Nanodiamond-Reinforced NiAl Nanocomposite Coating. *J. Therm. Spray Technol.* **2023**, *32*, 1299–1310. [CrossRef]
80. Xu, C.-A.; Liang, W.; Ni, C.; Li, X.; Shi, X.; Chu, Z.; Hu, Y.; Yang, Z. Silicone and nano-diamond modified graphene oxide anticorrosive coating. *Surf. Coat. Technol.* **2024**, *479*, 130584. [CrossRef]
81. Chen, C.; Yu, M.; Zhan, Z.; Ge, Y.; Sun, Z.; Liu, J. Dual strategy of improved crosslinking degree and incorporated inhibitory fillers for high corrosion resistance sol-gel coatings. *Corros. Sci.* **2024**, *234*, 112145. [CrossRef]
82. Chen, C.; Yu, M.; Xiao, J.; Jiang, M.; Liu, Y.; Wang, R.; Liu, J. One-step in-situ growth by one-pot method for uniform BTA@ZIF-8 layer to improve the corrosion protection of sol-gel coatings. *Corros. Sci.* **2025**, *250*, 112887. [CrossRef]
83. Liu, B.; Wang, Y.; Ji, Y.; Zou, M.; Wang, P.; Liu, S.; Ye, Q.; Zhou, F. Fabrication of Microgel-Functionalized Metal–Organic Framework Composite Polyurethane/Hydrogel Coatings with Enhanced Antifouling Performance. *ACS Appl. Mater. Interfaces* **2025**, *17*, 36009–36016. [CrossRef] [PubMed]
84. Ma, S.; Xu, J.; Sohrabi, S.; Zhang, J. Metal–organic gels and their derived materials for electrochemical applications. *J. Mater. Chem. A* **2023**, *11*, 11572–11606. [CrossRef]
85. Pérez-Almarcha, Y.; Martos, M.; Nacher-Luis, A.; Bosque, I.; Pastor, I.M. Metal–Organic Gels with Zirconium–Imidazolium Frameworks: A Versatile Platform for Eco-Friendly Organic Synthesis. *Chem.—Asian J.* **2025**, *20*, e00532. [CrossRef] [PubMed]
86. Oroujzadeh, A.R.; Nematollahzadeh, A.; Dabaleh, A.; Seifzadeh, D.; Shojaei, A. Fabrication of metal-organic gel (MOG) nanoparticles-enhanced epoxy coating as a pH-sensitive corrosion inhibitor under diverse environmental conditions. *Prog. Org. Coat.* **2025**, *209*, 109621. [CrossRef]

87. Akbarzadeh, S.; Batjargal, Z.; Ölmez, V.; Olivier, M.-G. Modified sol-gel layer incorporating hexagonal boron nitride (h-BN) nanosheets for improved corrosion resistance in plasma electrolytic oxidation coatings on AA2024. *Prog. Org. Coat.* **2025**, *200*, 109009. [CrossRef]
88. Kulyk, B.; Freitas, M.A.; Santos, N.F.; Mohseni, F.; Carvalho, A.F.; Yasakau, K.; Fernandes, A.J.S.; Bernardes, A.; Figueiredo, B.; Silva, R.; et al. A critical review on the production and application of graphene and graphene-based materials in anti-corrosion coatings. *Crit. Rev. Solid State Mater. Sci.* **2022**, *47*, 309–355. [CrossRef]
89. Zhang, M.; Wang, H.; Nie, T.; Bai, J.; Zhao, F.; Ma, S. Enhancement of barrier and anti-corrosive performance of zinc-rich epoxy coatings using nano-silica/graphene oxide hybrid. *Corros. Rev.* **2020**, *38*, 497–513. [CrossRef]
90. Habibpour, S.; Um, J.G.; Jun, Y.-s.; Bhargava, P.; Park, C.B.; Yu, A. Structural Impact of Graphene Nanoribbon on Mechanical Properties and Anti-corrosion Performance of Polyurethane Nanocomposites. *Chem. Eng. J.* **2021**, *405*, 126858. [CrossRef]
91. Akbarzadeh, S.; Akbarzadeh, K.; Ramezanzadeh, M.; Naderi, R.; Mahdavian, M.; Olivier, M.-G. Corrosion resistance enhancement of a sol-gel coating by incorporation of modified carbon nanotubes: Artificial neural network (ANN) modeling and experimental explorations. *Prog. Org. Coat.* **2023**, *174*, 107296. [CrossRef]
92. Afsharimani, N.; Durán, A.; Galusek, D.; Castro, Y. Hybrid Sol–Gel Silica Coatings Containing Graphene Nanosheets for Improving the Corrosion Protection of AA2024-T3. *Nanomater.* **2020**, *10*, 1050. [CrossRef] [PubMed]
93. Li, T.; Li, L.; Qi, J.; Chen, F. Corrosion protection of Ti6Al4V by a composite coating with a plasma electrolytic oxidation layer and sol-gel layer filled with graphene oxide. *Prog. Org. Coat.* **2020**, *144*, 105632. [CrossRef]
94. Nezamdoust, S.; Seifzadeh, D.; Habibi-Yangjeh, A. Nanodiamond incorporated sol−gel coating for corrosion protection of magnesium alloy. *Trans. Nonferrous Met. Soc. China* **2020**, *30*, 1535–1549. [CrossRef]
95. Verma, P.; Bannon, M.S.; Kuenen, M.K.; Raj, S.; Dhakal, A.; Stone, K.; Nichols, A.W.; Machan, C.W.; Colón, Y.J.; Letteri, R.A.; et al. Expanding the Design Space of Polymer–Metal Organic Framework (MOF) Gels by Understanding Polymer–MOF Interactions. *Chem. Mater.* **2024**, *36*, 9356–9369. [CrossRef] [PubMed]
96. Zhuang, Z.; Mai, Z.; Wang, T.; Liu, D. Strategies for conversion between metal–organic frameworks and gels. *Coord. Chem. Rev.* **2020**, *421*, 213461. [CrossRef]
97. Liu, Z.; Navas, J.L.; Han, W.; Ibarra, M.R.; Kwan, J.K.C.; Yeung, K.L. Gel transformation as a general strategy for fabrication of highly porous multiscale MOF architectures. *Chem. Sci.* **2023**, *14*, 7114–7125. [CrossRef] [PubMed]
98. Zhang, Y.; Wang, J.; Zhao, S.; Serdechnova, M.; Blawert, C.; Wang, H.; Zheludkevich, M.L.; Chen, F. Double-Ligand Strategy to Construct an Inhibitor-Loaded Zn-MOF and Its Corrosion Protection Ability for Aluminum Alloy 2A12. *ACS Appl. Mater. Interfaces* **2021**, *13*, 51685–51694. [CrossRef] [PubMed]
99. Wang, Y.; Hu, J.; Huang, H.; Zhang, T.; Wang, H.; Wang, A.; Li, T.; Hou, P.; Wei, J.; Yu, Q. Effect of metal-organic framework corrosion inhibitors on the micro/global properties of fresh and hardened cement paste. *Constr. Build. Mater.* **2026**, *506*, 145046. [CrossRef]
100. Schiller, C.A.; Strunz, W. The evaluation of experimental dielectric data of barrier coatings by means of different models. *Electrochim. Acta* **2001**, *46*, 3619–3625. [CrossRef]
101. Mohammadpour, Z.; Zare, H.R. The role of embedded 2-ABT@Cu-BTC MOF on the anti-corrosion performance of electro-assisted deposited silica sol-gel composite film. *Mater. Chem. Phys.* **2021**, *267*, 124590. [CrossRef]
102. Yimyai, T.; Crespy, D.; Rohwerder, M. Corrosion-Responsive Self-Healing Coatings. *Adv. Mater.* **2023**, *35*, 2300101. [CrossRef] [PubMed]
103. Paul, S.; Kaushik, A.K.; Jain, A.; Banerjee, S. Intelligent Self-Healing Polymeric Systems for Functional and Durable Coatings. *Chem.—Asian J.* **2026**, *21*, e70290. [CrossRef] [PubMed]
104. Wang, Z.; Sun, P.; Fan, Y.; Han, Y.; Hu, Y. Self-healing and rebar corrosion performance of cracked engineered cementitious composites exposed to wet coral sand environment. *Cem. Concr. Compos.* **2024**, *145*, 105372. [CrossRef]
105. Xu, C.; Zhang, Z.; Kasneryk, V.; Zeng, D.; Hu, J.; Wen, S.; Wang, Q.; Zhang, Y. Early-stage corrosion sensing via sequential fluorescence from sol-gel and ZnO layers: Self-healing ZIF-8 film-based composite coatings for aluminum alloys. *Corros. Sci.* **2026**, *263*, 113705. [CrossRef]
106. Chai, Y.; Sierra-Fernández, A.; Knez, M. Strategies, Challenges, and Future Prospects for Selective Corrosion Removal in Bronze and Copper-Based Alloys. *Adv. Funct. Mater.* **2026**, *36*, e75183. [CrossRef]
107. Lahrache, N.; Bouiti, K.; Bouhouche, I.; Labjar, N.; Nasrellah, H.; Laasri, S.; Cherrat, A.; El Hajjaji, S. Role of Nanotechnology in Concrete Corrosion Prevention. In *Corrosion in Concrete Structures*; Wiley: Hoboken, NJ, USA, 2026; pp. 317–341. [CrossRef]
108. Liu, X.; Li, J.; Li, S.; He, C.; He, H. Carbon Dots for Corrosion Protection: A Systematic Review of Applications and Mechanisms. *Nanomater* **2026**, *16*, 488. [CrossRef] [PubMed]
109. Guo, H.; Zhu, C.; Yuan, Z.; Huang, G.; Liang, H.; Xiong, C.; Feng, Z.; Wei, Q.; Meng, G. Facile Hydrogels of AIEgens Applied as Reusable Sensors for In Situ and Early Warning of Metallic Corrosion. *ACS Appl. Mater. Interfaces* **2023**, *15*, 8530–8536. [CrossRef] [PubMed]

110. Liu, Q.; Zhou, J.; Shen, Z.; Li, N.; Xie, S.; You, B.; Wu, L. Bio-Based Self-Healing Anti-Corrosion Coating with Gel Microspheres via One-Step In-Situ Crosslinking. *J. Colloid Interface Sci.* **2025**, *697*, 137795. [CrossRef] [PubMed]
111. Chen, Y.; Wang, Q.; Hou, L.; Huang, H.; Gao, Z.; Wei, Y. Self-Warning and Self-Repairing Mechanisms in Functional Coatings: A Review. *Exploration* **2025**, *5*, e20240066. [CrossRef] [PubMed]
112. Wang, M.; Jiang, G.; Zhou, J.; Wang, Q.; Zhang, C.; Zhao, D. Bio-Based Polymer Gels: Molecular-Macroscopic Functional Design and Promising Applications in Wearable Flexible Sensing. *Macromol. Rapid Commun.* **2025**, *n/a*, e00695. [CrossRef] [PubMed]
113. Liu, B.; Zhang, S.; Zhao, L.; Zou, C.; Xiu, J. Multifunctional Bio-Gels in Environmental Remediation: Current Advances and Future Perspectives. *Gels* **2025**, *11*, 864. [CrossRef] [PubMed]
114. Kervancıoğlu, G.; Gürsel Sürmelioğlu, D. The Effect of Home Bleaching Gel with Chitosan on Tooth Color and Mineral Alteration. *Gels* **2025**, *11*, 933. [CrossRef] [PubMed]
115. Akbarzadeh, S.; Coelho, L.B.; Dangreau, L.; Lanzutti, A.; Fedrizzi, L.; Olivier, M.-G. Self-healing plasma electrolytic oxidation (PEO) coating developed by an assembly of corrosion inhibitive layer and sol-gel sealing on AA2024. *Corros. Sci.* **2023**, *222*, 111424. [CrossRef]
116. Zhang, H.; Lin, B.; Tang, J.; Wang, Y.; Wang, H.; Zhang, H.; Cao, J.; Hou, J.; Sun, M.; Zhang, H. An ethyl cellulose-based supramolecular gel composite coating for metal corrosion protection and its self-healing property from electromagnetic heating effect. *Surf. Coat. Technol.* **2021**, *424*, 127647. [CrossRef]
117. Xu, P.; Wang, X.; Wang, T.; Zhao, X.; Tan, J.; Ge, W.; Zhang, B.; Meng, G. Synergetic Inhibition and Corrosion-Sensing Abilities Based on pH-Sensitive ZIF-8@CeO2 Core–Shell Nanocontainers toward Intelligent Coating. *ACS Appl. Mater. Interfaces* **2026**, *18*, 6064–6077. [CrossRef] [PubMed]
118. Kim, C.; Karayan, A.I.; Milla, J.; Hassan, M.; Castaneda, H. Smart Coating Embedded with pH-Responsive Nanocapsules Containing a Corrosion Inhibiting Agent. *ACS Appl. Mater. Interfaces* **2020**, *12*, 6451–6459. [CrossRef] [PubMed]
119. Li, Y.; Wang, J.; Liu, S. Synthesis of Temperature/pH Dual-Responsive Double-Crosslinked Hydrogel on Medical Titanium Alloy Surface. *Gels* **2025**, *11*, 443. [CrossRef] [PubMed]
120. Samadianfard, R.; Seifzadeh, D.; Dikici, B. Smart sol-gel nanocomposite containing inhibitor-stabilized g-C3N4 nanoplates for corrosion protection of magnesium alloy. *Surf. Coat. Technol.* **2024**, *484*, 130764. [CrossRef]
121. Fang, B.; Zhang, X.; Liu, H.; Zhao, F.; Li, Y.; Zeng, X.; Feng, Z.; Li, W.; Liu, J. Improved anti-corrosion performance of epoxy coatings based on pH-sensitive gels loaded with inhibitors. *J. Mater. Res. Technol.* **2025**, *34*, 1682–1690. [CrossRef]
122. Shitanda, I.; Okamoto, Y.; Loew, N.; Nagamine, K.; Watanabe, H.; Matsuhisa, N.; Itagaki, M. Flexible sticker-type three-electrode device with PVA gel electrolyte for on-site electrochemical corrosion evaluation. *Electrochim. Acta* **2025**, *543*, 147590. [CrossRef]
123. Chen, J.; Dong, Z.; Li, M.; Li, X.; Chen, K.; Yin, P. Ultra-Strong and Proton Conductive Aqua-Based Adhesives from Facile Blending of Polyvinyl Alcohol and Tungsten Oxide Clusters. *Adv. Funct. Mater.* **2022**, *32*, 2111892. [CrossRef]
124. Hu, R.; Zhao, J.; Wang, Y.; Li, Z.; Zheng, J. A highly stretchable, self-healing, recyclable and interfacial adhesion gel: Preparation, characterization and applications. *Chem. Eng. J.* **2019**, *360*, 334–341. [CrossRef]
125. Pan, T.; Wang, X.; Mao, L.; Wang, H. Highly adhesive and conductive eco-friendly Mg/B-SA/PVA ionogels. *Chem. Eng. J.* **2025**, *522*, 167816. [CrossRef]
126. Daniyal, M.; Akhtar, S. Corrosion assessment and control techniques for reinforced concrete structures: A review. *J. Build. Pathol. Rehabil.* **2019**, *5*, 1. [CrossRef]
127. Haufe, M.; Bakalli, M.; Sahin, H.; Helm, C.; Achenbach, R. Newly developed acrylate injection resin gels for structural sealing and active corrosion protection of embedded steel reinforcement. *Mater. Corros.* **2020**, *71*, 824–833. [CrossRef]
128. Zhang, T.; Dai, Y.; Ren, S.; Huang, Z.; Han, C.; Ding, W. Polymer–Silicate Composite Gel Systems for Enhanced Chloride Resistance of Cement-Based Materials. *Gels* **2025**, *11*, 936. [CrossRef] [PubMed]
129. Chen, W.; Liu, Y.; Qian, H.; Wu, P.; Wu, Y.; Liu, F. Chloride Ion Corrosion Resistance of Innovative Self-Healing SMA Fiber-Reinforced Engineering Cementitious Composites under Dry-Wet Cycles for Ocean Structures. *Buildings* **2023**, *13*, 518. [CrossRef]
130. Naidu Gopu, G.; Joseph, S.A. Corrosion Behavior of Fiber-Reinforced Concrete—A Review. *Fibers* **2022**, *10*, 38. [CrossRef]
131. Fuhaid, A.F.; Niaz, A. Carbonation and Corrosion Problems in Reinforced Concrete Structures. *Buildings* **2022**, *12*, 586. [CrossRef]
132. Xu, P.; Jia, Q. Evaluation the mechanical and electrochemical anti-corrosion properties of polydimethylsiloxane/SiO2 gel coated carbon steel rebar in concrete pore solution. *Int. J. Electrochem. Sci.* **2023**, *18*, 100043. [CrossRef]
133. Zhang, M. Crack-free Sol-Gel Coatings for Corrosion Protection of Carbon steel in concrete pore solution: An electrochemical corrosion investigation. *Int. J. Electrochem. Sci.* **2021**, *16*, 211026. [CrossRef]
134. Jung, A.; Weichold, O. A 3-in-1 alkaline gel for the crack injection in cement-based materials with simultaneous corrosion protection and re-passivation of crack-crossing steel rebars. *Constr. Build. Mater.* **2022**, *344*, 128092. [CrossRef]
135. Domínguez-Martínez, J.; López-Sánchez, J.; García-Galván, F.; Serrano, A.; Barranco, V.; Galván, J.C.; Rodríguez de la Fuente, Ó.; Carmona, N. Eco-Friendly Sol–Gel Coatings with Organic Corrosion Inhibitors for Lightweight AZ61 Alloy. *Gels* **2024**, *10*, 168. [CrossRef] [PubMed]

136. Rikhari, B.; Rani, B.E.A. Sustainable corrosion protection of aluminium alloys using a bio-based carbohydrate inhibitor. *Surf. Coat. Technol.* **2025**, *513*, 132475. [CrossRef]
137. Rajimol, P.R.; Ulaeto, S.B.; Athira, R.V.; Puthiyamadam, A.; Sahoo, S.K.; Rajan, T.P.D.; Radhakrishnan, K.V.; Sukumaran, R.K. Development of an oxyresveratrol incorporated bio-based smart nanocomposite coating with anti-corrosive, self-healing, and anti-microbial properties. *Green Chem.* **2023**, *25*, 7189–7215. [CrossRef]
138. Eral, S.; Oktay, B.; Dizman, C.; Kayaman Apohan, N. Preparation of organic–inorganic bio-based epoxy coatings with high anti-corrosive performance. *Polym. Bull.* **2024**, *81*, 6873–6890. [CrossRef]
139. Purwasena, I.A.; Karima, A.; Asri, L.A.T.W.; Setiawan, A.R. The potency of spores and biosurfactant of Bacillus clausii as a new biobased sol-gel coatings for corrosion protection of carbon steel ST 37 in water cooling systems. *Appl. Surf. Sci. Adv.* **2023**, *18*, 100452. [CrossRef]
140. Ghuzali, N.A.M.; Noor, M.A.A.C.M.; Zakaria, F.A.; Hamidon, T.S.; Husin, M.H. Study on Clitoria ternatea extracts doped sol-gel coatings for the corrosion mitigation of mild steel. *Appl. Surf. Sci. Adv.* **2021**, *6*, 100177. [CrossRef]
141. Sheydaei, M.; Edraki, M.; Radeghi Mehrjou, S.M. Anticorrosion and Antimicrobial Evaluation of Sol-Gel Hybrid Coatings Containing Clitoria ternatea Modified Clay. *Gels* **2023**, *9*, 490. [CrossRef] [PubMed]
142. Hamidon, T.S.; Hussin, M.H. Susceptibility of hybrid sol-gel (TEOS-APTES) doped with caffeine as potent corrosion protective coatings for mild steel in 3.5 wt.% NaCl. *Prog. Org. Coat.* **2020**, *140*, 105478. [CrossRef]
143. Motalebi, A.; Nasr-Esfahani, M.; Ali, R.; Pourriahi, M. Improvement of corrosion performance of 316L stainless steel via PVTMS/henna thin film. *Prog. Nat. Sci. Mater. Int.* **2012**, *22*, 392–400. [CrossRef]
144. Ulaeto, S.B.; Mathew, G.M.; Pancrecious, J.K.; Rajimol, P.R.; Karun, A.S.; Rajan, T.P.D. Azadirachta indica (Neem) self-healing efficacy assessment in epoxy primer coatings: A bio-responsive strategy for counteracting corrosion. *Colloids Surf. A Physicochem. Eng. Asp.* **2023**, *658*, 130684. [CrossRef]
145. Das, P.; Sharma, N.; Puzari, A.; Kakati, D.K.; Devi, N. Synthesis and characterization of neem (Azadirachta indica) seed oil-based alkyd resins for efficient anticorrosive coating application. *Polym. Bull.* **2021**, *78*, 457–479. [CrossRef]
146. Edraki, M.; Zaarei, D.; Sabeeh Hasan, I. The Impact of Green Corrosion Inhibitors on the Protection Performance of Hybrid Silane Sol-Gel Coatings: A Review. *Chem. Rev. Lett.* **2023**, *6*, 428–441. [CrossRef]
147. Cambero, E.R.; Viñuales, A.I.; Altube, A.; Labidi, J.; Erdocia, X.; Aparicio, X.; Grande, H.-J.; García-Lecina, E. A Sustainable and Room Temperature Curable Sol–Gel Formulation for the Preparation of Corrosion Resistant Hybrid Coatings Cross-Linked with Lignin. *ACS Sustain. Chem. Eng.* **2026**, *14*, 1926–1939. [CrossRef]

Disclaimer/Publisher's Note: The statements, opinions and data contained in all publications are solely those of the individual author(s) and contributor(s) and not of MDPI and/or the editor(s). MDPI and/or the editor(s) disclaim responsibility for any injury to people or property resulting from any ideas, methods, instructions or products referred to in the content.